

Shown LEFT is Planet's Fusion Monitoring Product (PlanetScope data)  
Shown RIGHT is LandSat 8 data of the same area



# PLANET FUSION MONITORING TECHNICAL SPECIFICATION

## SURFACE REFLECTANCE

Version 1.3.0, June 2024



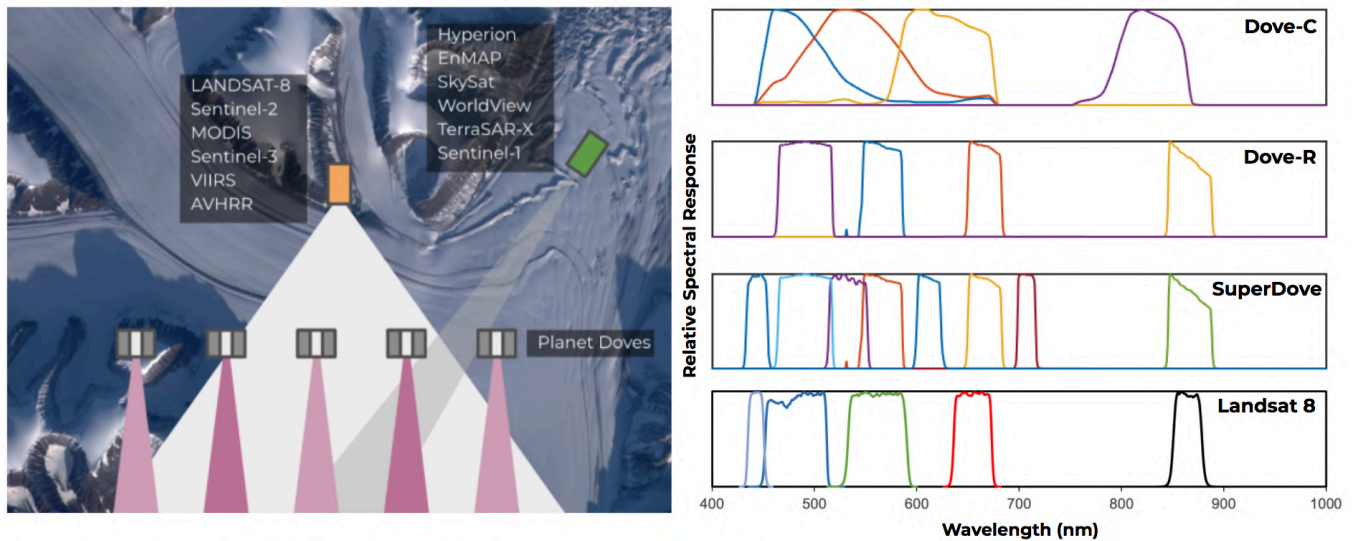
# TABLE OF CONTENTS

<b>TABLE OF CONTENTS</b>	<b>2</b>
<b>1. PLANET FUSION OVERVIEW</b>	<b>3</b>
<b>2. PLANET FUSION INPUTS</b>	<b>5</b>
<b>3. PLANET FUSION PRODUCTS</b>	<b>6</b>
3.1. SURFACE REFLECTANCE PRODUCT (PF-SR)	7
3.2. QUALITY ASSURANCE PRODUCT (PF-QA)	7
3.3. SPATIOTEMPORAL ASSET CATALOG (STAC)	10
3.4. PROJECTION, GRIDDING, FILE NAMING, AND DELIVERY	11
<b>4. PLANET FUSION METHODOLOGY</b>	<b>12</b>
4.1. TILE (CHUNK)-LEVEL STACKING	13
4.2. TOPOGRAPHIC CORRECTION	14
4.3. CLOUD AND CLOUD SHADOW MASKING	15
4.4. REFERENCE SAMPLING AND RADIOMETRIC HARMONIZATION	16
4.5. GEOMETRIC HARMONIZATION	18
4.6. GAP-FILLING	19
4.6.1. Predictive feature	22
4.7. TEMPORAL FILTERING	23
4.8. CONFIDENCE INFORMATION	24
4.9. BACKFILL VERSUS FORWARD-FILL OPERATION	26
4.10. PIXEL RESOLUTION DEPENDENT DATA FUSION OPTIONS	26
<b>5. QUALITY MONITORING</b>	<b>29</b>
5.1. RADIOMETRIC VALIDATION	29
5.2. GEOMETRIC VALIDATION	34
5.3. CLOUD MASK PERFORMANCE	36
5.4. GAP-FILLING PERFORMANCE	37
<b>6. KNOWN LIMITATIONS AND CAVEATS</b>	<b>40</b>
<b>REFERENCES</b>	<b>41</b>

# 1. PLANET FUSION OVERVIEW

The PlanetScope constellation of 180+ CubeSats in low earth orbits represents a novel observational resource, which when combined with advances in conventional spaceborne sensing has resulted in a proliferation of satellite sensor data with unprecedented spatial, temporal, and spectral resolution. This constitutes a revolution in the ability to derive time-critical, location-specific insights about dynamic land surface processes. However, the potential for these systems to support decision making is often limited by sensor interoperability issues (Figure 1), cross-calibration challenges, and atmospheric contamination. These obstacles can stand in the way of realizing the full potential of these rich datasets.

Figure 1: Sources of interoperability issues. Left: The reflectance field of the same observation target can appear very different at the point of the satellite sensor due to differences in satellite viewing and sun illumination angles augmented by shadow effects and non-lambertian surface characteristics (i.e., as described by the Bidirectional Reflectance Distribution Function; BRDF). Right: Differences in spectral bands and spectral response functions can result in poor sensor interoperability. This is particularly pronounced when comparing Dove-C (i.e., first generation PlanetScope) with public sensor sources (e.g., L8).

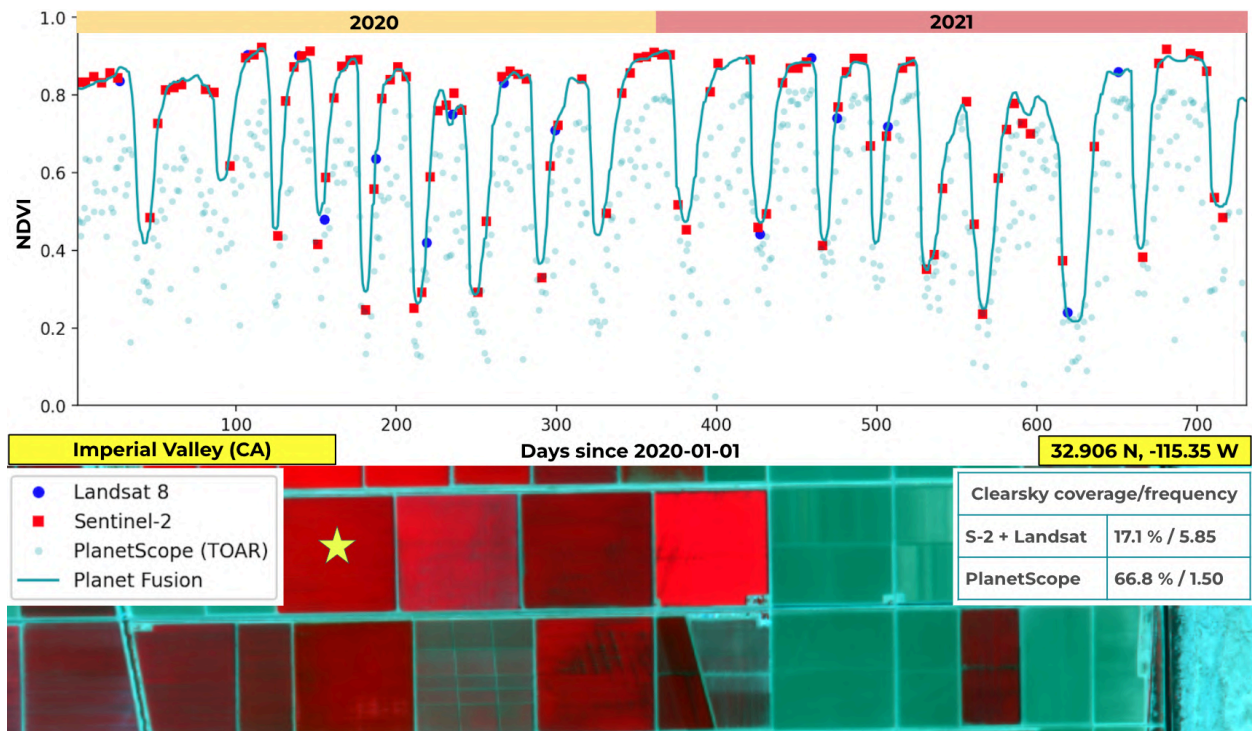


At Planet, we have implemented and improved a rigorous methodology to enhance, harmonize, inter-calibrate, and fuse cross-sensor data streams. The CubeSat-Enabled Spatio-Temporal Enhancement Method (CESTEM) (Houborg and McCabe 2018a, 2018b) leverages rigorously calibrated publicly accessible multispectral satellites (i.e., Sentinel, Landsat, MODIS, VIIRS) to work in concert with the higher spatial and temporal resolution data provided by Planet’s Dove CubeSats. The result is a next generation, analysis ready, harmonized Level-3 data product, which delivers a clean (i.e. free from clouds and shadows), gap-filled (i.e., daily, 3 m), temporally consistent, and radiometrically accurate 4-band surface reflectance (SR) data product.

Planet Fusion integrates all of the best features from both public and private satellite sensor resources. Distributed observations from multiple sensors with differing radiometry, quality, and spatiotemporal resolution characteristics are condensed and harmonized into a usable sensor-agnostic dataset that inherits the best traits from each sensor while ensuring radiometric consistency with a suite of widely used “reference” satellite platforms. This next generation Analysis Ready Data (ARD) product is suitable for analytic and data science purposes and has proven particularly beneficial for inter-day change detection and disturbance monitoring, dynamic land use and land cover classification, phenology and vegetation growth monitoring, and biophysical properties and process retrievals (e.g., Aragon et al., 2021; Nieto et al., 2022; Brinkhoff et al., 2022; Johansen et al., 2022; Ziliani et al., 2022; Kong et al., 2022 & 2023; Luo et al., 2023). Planet Fusion involves significant processing

and novel methodology in the attempt to create a unique Surface Reflectance product enhanced in resolution, quality, and interoperability (Figure 2), as the pathway to useability and meaningful remote sensing driven insights.

Figure 2: Normalized Difference Vegetation Index (NDVI) time series over a dynamic multi-cut alfalfa field in Imperial Valley (CA) over the course of two years (2020 - 2021). The Planet Fusion processing translates original PS Top Of Atmosphere (TOA) reflectance inputs into Surface Reflectances (SR) consistent with Landsat 8/9 and Sentinel-2 clear-sky observations. Gaps in the Planet Fusion time series (due to clouds, missing acquisition data) have been filled using an elaborate gap-filling and data fusion technique (Section 4.6) to provide a spatially complete daily product. Note the bump up in in clearsky revisit frequency from 5.85 (Sentinel-2 and Landsat 8) to 1.5 when incorporating PlanetScope observations over this AOI.



The unique features of Planet Fusion data can be summarized as:

- **Advanced radiometric harmonization which leverages rigorously calibrated third-party sensors (MODIS/VIIRS, Landsat 8/9, and Sentinel-2) for full fleet interoperability**
- **Rigorous, temporally driven, cloud and cloud shadow detection**
- **Cleaned and gap-filled (daily) Surface Reflectance values delivered as regularly gridded UTM raster tiles (24 km x 24 km) with a 48 hour latency**
- **Fusion of Sentinel-2 and Landsat 8/9 data to help fill gaps in PlanetScope coverage**
- **CubeSats with near-nadir field of view result in minimal BRDF variation effects**
- **Designed to provide high radiometric accuracy and spatio-temporal consistency**
- **Geometric harmonization with sub-pixel co-registration/alignment of disparate image sources**
- **Includes pixel traceability information to easily identify source imagery and assess the confidence of gap-filled data for every data point**

## 2. PLANET FUSION INPUTS

[Table 1](#) lists the data sources currently used in Planet Fusion production.

Planet's collection of 180+ CubeSats operate in sun synchronous orbits (altitude ~475 km) with a midmorning equatorial overpass time (9:30–11:30 a.m., local solar time) providing global near-nadir (~4° field of view) imaging on a near-daily basis ([Roy et al., 2021](#)). Three generations of “Doves” are used as input to Planet Fusion products; the Dove-Classic constellation (2016–2022) is characterized by broad and partly overlapping spectral bands in the visible and near-infrared (NIR) spectrum ([Figure 1](#)), whereas the Dove-R (2019–2022) and SuperDove (2020–) constellations are improved to be directly interoperable with the visible and narrow NIR bands of Sentinel-2. The nominal ortho scene size (at 475 km altitude) is also larger for Dove-R (~25 km x 23 km) and SuperDove (~32.5 km x 19.6 km) relative to Dove-Classic (~25 km x 11.5 km). PlanetScope Top Of Atmosphere (TOA) Radiance inputs contribute the bulk of the observations used to make Fusion, and they are derived from 4-band Orthorectified Scene Products that have a resampled pixel size of 3 m (i.e., the ground sampling distance is altitude dependent and ranges from 3.0 to 4.2 m). While the SuperDove is an 8-band sensor (i.e., adds bands in the visible and red-edge domain), currently only the blue, green, red, and NIR bands are used in Planet Fusion production.

Table 1: List of inputs currently used in Planet Fusion production.

Product	Description
PS-TOA	Scene-based PlanetScope Top Of Atmosphere (TOA) Radiance (4-band, 3 m) ( <a href="https://assets.planet.com/docs/Planet_PSScene_Imagery_Product_Spec_letter_screen.pdf">https://assets.planet.com/docs/Planet_PSScene_Imagery_Product_Spec_letter_screen.pdf</a> )
MCD43A4, MCD43A4N	Tile-based MODIS Surface Reflectance (SR) normalized to a nadir view direction and local solar noon (daily, 500 m) ( <a href="https://lpdaac.usgs.gov/products/mcd43a4v061/">https://lpdaac.usgs.gov/products/mcd43a4v061/</a> )
VNP43IA4, VNP43IA4N	Tile-based SR (VIIRS imagery bands) normalized to a nadir view direction and local solar noon (daily, 500 m) ( <a href="https://lpdaac.usgs.gov/products/vnp43ia4v001/">https://lpdaac.usgs.gov/products/vnp43ia4v001/</a> )
VNP43MA4, VNP43MA4N	Tile-based SR (VIIRS moderate bands) normalized to a nadir view direction and local solar noon (daily, 1000 m) ( <a href="https://lpdaac.usgs.gov/products/vnp43ma4v001/">https://lpdaac.usgs.gov/products/vnp43ma4v001/</a> )
FLS-SR	In-house implementation for tile-based generation of Nadir BRDF Adjusted Reflectances (NBAR) from Landsat 8/9 and Sentinel-2 data (4-band, 30 m). The Landsat 8/9 data have been spectrally adjusted to match Sentinel-2 spectral band passes. Based on the Framework for Operational Radiometric Correction for Environmental Monitoring (FORCE) ( <a href="https://github.com/davidfrantz/force">https://github.com/davidfrantz/force</a> )

We use a scalable implementation of the Framework for Operational Radiometric Correction for Environmental Monitoring (FORCE version 3.7.7; [Frantz 2019a](#)) for generating a combined Landsat 8/9 (L8/9) and Sentinel-2 (S-2) surface reflectance product (FLS-SR) to be used as the “gold reference” during the radiometric calibration and normalization of Planet Fusion products. FORCE includes state-of-the-art atmospheric correction, topography/terrain correction, cloud and cloud shadow detection, spatial co-registration, and view angle normalization ([Frantz 2019a](#)). FORCE infers surface reflectance from Landsat 8/9 and Sentinel-2 imagery using an implementation of the 5S (Simulation of the Satellite Signal in the Solar Spectrum) code ([Tanre et al., 1990](#)). The aerosol optical depth is estimated from the imagery using a dark object based approach whereas the water vapor content is either estimated on a pixel-specific basis (S-2) or derived from a global MODIS-based database (L8/9) ([Frantz et al., 2019b](#)). Clouds and cloud shadows are detected using a modified version of Fmask ([Zhu and Woodcock, 2012](#)) that exploits parallax effects to improve detections for S-2 images ([Frantz et al., 2018](#)). However the FORCE derived cloud masks may be further refined as part of Fusion processing ([Section 4.3](#)). A global

assessment of the FORCE atmospheric correction approach has been conducted as part of the Atmospheric Correction Inter-comparison Exercises (ACIX, ACIX-II) ([Doxani et al., 2018](#) & [2023](#)).

Our FORCE implementation maps the L8/9 and S-2 data onto a common grid (i.e., the UTM-based Military Grid Reference System) to produce 30 m resolution L8/9 and S-2 data with a 2 - 3 day frequency. A spectral bandpass adjustment ([Claverie et al. 2018](#)) is applied to L8/9 to align with S-2 radiometry. Only the blue (center wl: 0.490  $\mu\text{m}$ , bandwidth: 0.065  $\mu\text{m}$ ), green (center wl: 0.560  $\mu\text{m}$ , bandwidth: 0.035  $\mu\text{m}$ ), red (center wl: 0.665  $\mu\text{m}$ , bandwidth: 0.030  $\mu\text{m}$ ), and narrow NIR (center wl: 0.865  $\mu\text{m}$ , bandwidth: 0.021  $\mu\text{m}$ ) bands (S-2 radiometry) are currently used for the Planet Fusion production. The reported bandwidths are the values measured at Full Width Half Maximum (FWHM).

MODIS or VIIRS surface reflectance (SR) data normalized to nadir view and local solar noon is a required input to the Planet Fusion reference sampling and calibration process ([Section 4.4](#)). Planet Fusion uses the version 6.1 combined (i.e., Terra and Aqua) MCD43A4 product that provides daily 500 m SR in 7 bands corrected for reflectance anisotropy (MODIS has a  $\sim 110^\circ$  field of view) using a semiempirical bidirectional reflectance distribution function (BRDF) ([Schaaf et al. 2002](#)). The BRDF utilizes the best observations from both Terra and Aqua sensors collected over a 16-day period centered on the day of interest where observations at the day of interest are emphasized in the daily retrieval. Only the blue (0.459 - 0.479  $\mu\text{m}$ ), green (0.545 - 0.565  $\mu\text{m}$ ), red (0.62 - 0.67  $\mu\text{m}$ ), and NIR (0.841 - 0.876  $\mu\text{m}$ ) bands are ingested for Planet Fusion processing. The near real-time product version (MCD43A4N) is used when the standard product isn't available (i.e., as dictated by a 9 days latency). The VIIRS products (VNP43IA4/VNP43IA4N, VNP43MA4/VNP43MA4N) have been designed to ensure continuity of MCD43 and are used as a backup should MCD43A4/MCD43A4N become unavailable. The VIIRS-based processing ingests the red (0.60 - 0.68  $\mu\text{m}$ ) and NIR (0.85 - 0.88  $\mu\text{m}$ ) Imagery bands (500 m) in addition to the blue (0.478 - 0.488  $\mu\text{m}$ ) and green (0.545 - 0.565  $\mu\text{m}$ ) Moderate bands (1000 m). Since the two latter bands are provided at a coarser spatial resolution (1000 m), the finer resolution (500 m) red band is used to super-resolve the data for consistency.

### 3. PLANET FUSION PRODUCTS

The Planet Fusion (PF) product line is outlined in [Table 2](#). The Planet Fusion products are spatially complete (i.e., gap-free), cloud-free, provided at a daily cadence, and orthorectified onto a fixed grid (see [Section 3.4](#)) with a default 3 m pixel size (see [Section 4.10](#) for a description of other target pixel size options and associated data fusion scenarios). The products can be produced starting from January 1, 2017 and up till present, deliverable with a 48 hour latency (i.e., data requested for Monday will be delivered Wednesday).

Table 2: Overview descriptions of the Planet Fusion (PF) products.

Product key	Description
PF-SR	Planet Fusion Surface Reflectance (SR) product. PS TOA Reflectance radiometrically harmonized to 4-band FLS-SR using the CESTEM methodology. Cloud masked and gap-filled via PS, MODIS/VIIRS, Landsat 8/9, and Sentinel-2 data fusion (gap-free, daily, 3 m)
PF-QA	Planet Fusion Quality Assurance product
PF-STAC	Planet Fusion SpatioTemporal Asset Catalog items and catalog

### 3.1. SURFACE REFLECTANCE PRODUCT (PF-SR)

The Planet Fusion Surface Reflectance product (PF-SR) records gridded (3 m by default), radiometrically and geometrically corrected, and gap-free orthorectified data in four spectral bands (blue, green, red, NIR) at a daily interval. The data is stored in 16-bit integer format (with a multiplication factor of 10,000) as cloud optimized geotiffs compressed using LZW compression. During Planet Fusion processing and harmonization, 4-band PS TOA Reflectance (PS-TOAR) (converted from the radiances) are transformed into surface reflectances ensuring radiometric consistency with Sentinel-2. As a result the spectral bands and spectral response functions of Planet Fusion data ([Table 3](#)) will be equivalent to the blue (B2), green (B3), red (B4), and narrow NIR (B8a) bands of Sentinel-2 ([ESA 2024](#)).

The Planet Fusion SR data represent Normalized BRDF Adjusted Reflectances (NBAR) as the Landsat 8/9 and Sentinel-2 data used for cross-calibration have been normalized to nadir view ([Roy et al. 2016, 2017](#)). As the Planet Fusion cross-calibration adopts a multi-temporal reference sampling approach (see [Section 4.4](#)), the significant uncertainties related to the L8/L9/S-2-based BRDF normalization ([Roy et al. 2017](#)) are likely to cancel out. In addition, in contrast to L8/9 (~15° field of view) and particularly S-2 (~21° field of view), the PlanetScope sensors are nadir viewing natively (~4° field of view), which will act to further minimize view angle BRDF effects.

Table 3: PF-SR data format specifications providing the band-specific center wavelengths and bandwidths (bw). The bandwidths are the values measured at FWHM.

Layer	Description	Date Type	Valid range	Scale factor
Band 1	Blue band (0.490 μm, bw: 0.065 μm) SR (NBAR)	16-bit signed integer	1 - 10,000	0.0001
Band 2	Green band (0.560 μm, bw: 0.035 μm) SR (NBAR)	16-bit signed integer	1 - 10,000	0.0001
Band 3	Red band (0.665 μm, bw: 0.030 μm) SR (NBAR)	16-bit signed integer	1 - 10,000	0.0001
Band 4	NIR band (0.865 μm, bw: 0.021 μm) SR (NBAR)	16-bit signed integer	1 - 10,000	0.0001

### 3.2. QUALITY ASSURANCE PRODUCT (PF-QA)

The Planet Fusion Quality Assurance (QA) product is a 9 layer thematic raster using the same spatial grid as the corresponding Planet Fusion spectral data. It contains information denoting gap-filling (layers 1 and 2), cloud and cloud shadow detection (layer 3), pixel traceability/provenance (layer 4), number of L8/L9/S-2 reference scenes used during calibration (layer 5), and spectral confidence estimates for synthetic (gap-filled) data (layer 6 - 9) ([Table 5](#)).

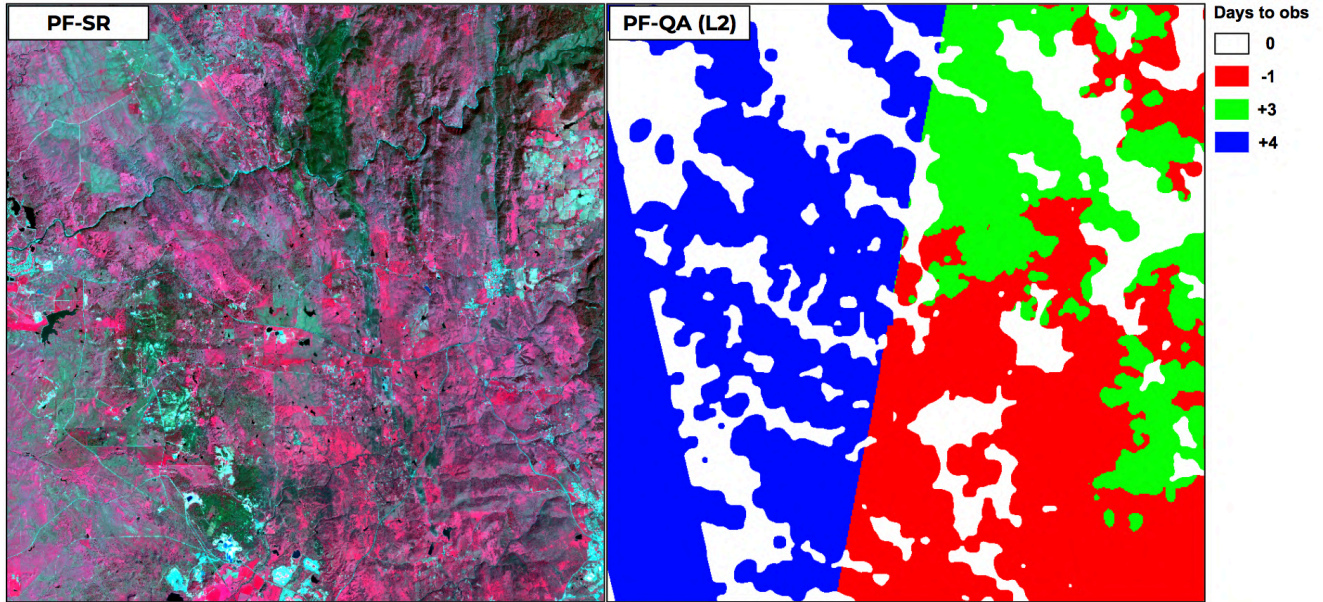
Table 5: PF-QA data format specifications. Note that additional metadata have been embedded in the tiff file, as described in the table

Layer	Description	Date Type	Valid range	Scale factor	Offset
Layer 1	Percentage of synthetic (gap-filled) versus actual PlanetScope data used to generate pixel value. A 100% synthetic pixel will have a value of 100.	16-bit signed integer	0 - 100	1	0

Layer 2	<p>Number of days to closest pixel-level observation used to gap-fill (- is before, + is after prediction day)</p> <p><i>See embedded metadata for the dates [yyyymmdd] of the closest imagery used to gap-fill</i></p> <p>900 (-900): Sentinel-2 (Landsat 8/9) data <b>acquired on the prediction day</b> used to inform gap-filling</p> <p><i>See embedded metadata for the scene IDs of the L8/L9/S-2 data (if any) used to inform gap-filling</i></p> <p>-999 = Gap-filling was unsuccessful</p>	16-bit signed integer	-900 to 900, and -999	1	0
Layer 3	<p>Cloud and cloud shadow mask</p> <p>1 = Clear</p> <p>2 = Bright Clouds</p> <p>3 = Cloud shadows</p> <p>4 = Haze</p> <p>5 = Adjacent clouds/clouds shadows</p> <p>6 = Additional cloud/shadow/haze elements based on a cross-scene correlation detection approach</p> <p>7 = Other contamination, including snow</p> <p>-999 = Scene data not available</p>	16-bit signed integer	1 - 7, and -999	1	0
Layer 4	<p>Pixel traceability/provenance mask (<i>see embedded metadata for scene IDs</i>)</p> <p>-999 = Scene data not available</p>	16-bit signed integer	1 - 599, and -999	1	0
Layer 5	<p>Total number of FORCE L8/L9/S-2 reference scenes used during calibration</p> <p>-999 = Scene data not available</p>	16-bit signed integer	0 - 500, and -999	1	0
Layer 6	Blue band uncertainty estimate (absolute percentage)	16-bit signed integer	3 - 200	1	0
Layer 7	Green band uncertainty estimate (absolute percentage)	16-bit signed integer	3 - 200	1	0
Layer 8	Red band uncertainty estimate (absolute percentage)	16-bit signed integer	3 - 200	1	0
Layer 9	NIR band uncertainty estimate (absolute percentage)	16-bit signed integer	3 - 200	1	0

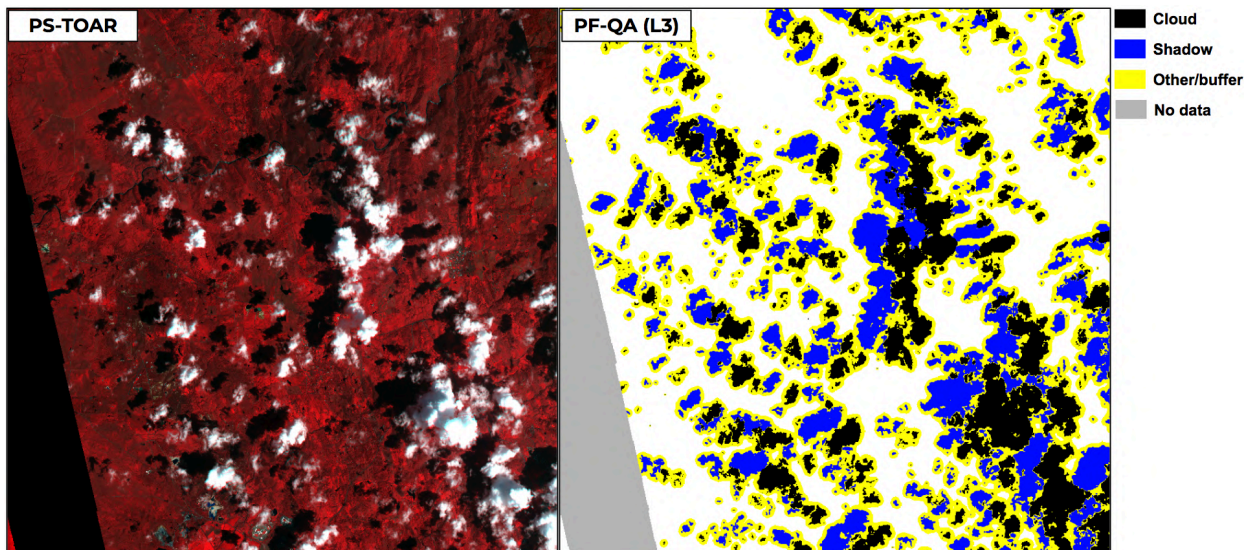
QA layer 1 represents a raster mask indicating the percentage of “synthetic” (i.e., gap-filled) versus observed PlanetScope data used to produce each pixel value across the tile domain. A value of 0 indicates no gap-filling (i.e., 100% observed PS data) whereas a value of 100 indicates an entirely (100%) gap-filled pixel value. The pixel-specific weighting (0 - 100) in the neighborhood of gaps is done to ensure smooth and gradual transitions across interfaces between synthetic and observed data points.

Figure 3: QA layer 2 (gap-filling confidence metric) and PF-SR product for a tile east of Sacramento (CA) on a day with significant cloud and cloud shadow contamination. In QA layer 2, pixels containing real observation data will have a value of 0, whereas synthetic (gap-filled) pixels will be represented by the number of days since a valid observation (a negative/positive day value indicates an observation acquired before/after the given day).



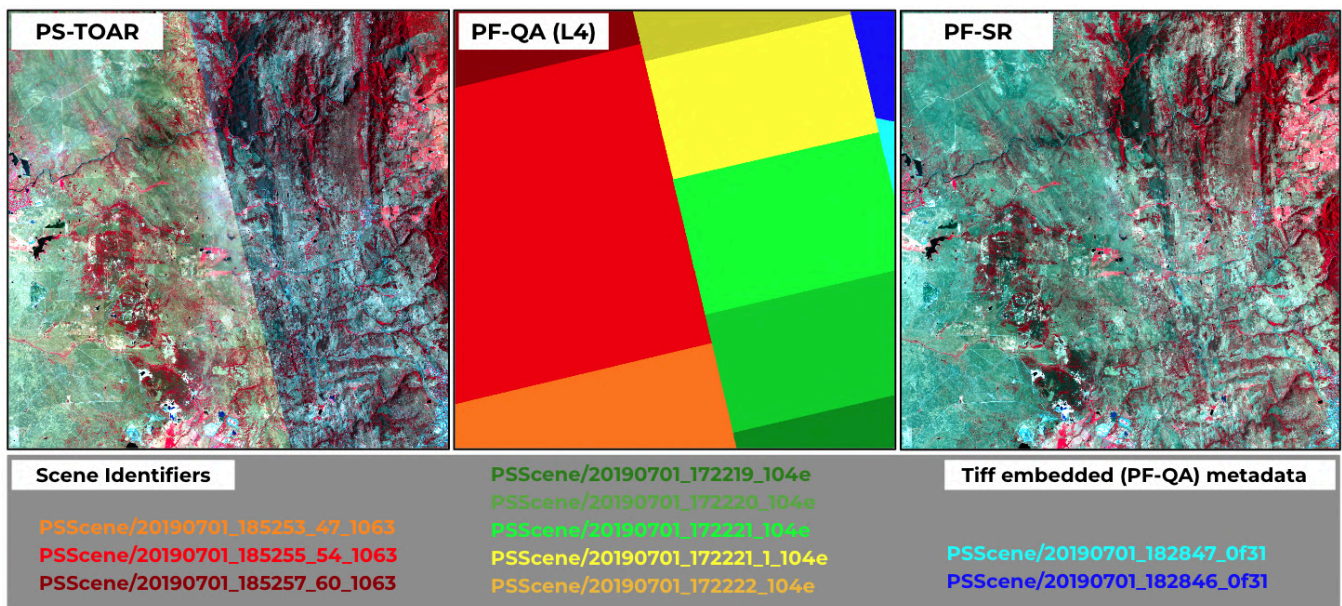
QA layer 2 is a metric of gap-filling confidence, represented by pixel-specific information on the number of days to a satellite acquisition with clear-sky observations. The longer the day gap, the higher the uncertainty is likely to be in the gap-filled estimate although several factors will play a role in the actual retrieval uncertainty (see [Section 4.8](#)). This QA layer will also identify pixels where FORCE-based L8/L9/S-2 SR data (FLS-SR) on the prediction date have been used to help fill gaps resulting from clouds or gaps in PlanetScope coverage ([Table 5](#)). The actual dates of the closest images used to gap-fill have been included as tiff embedded metadata. The embedded metadata will also store the scene identifiers of the Sentinel or Landsat data (if any) used to fill gaps in PS coverage. [Figure 3](#) exemplifies this metric for an AOI close to Sacramento (CA). [Figure 4](#) depicts the associated cloud and cloud shadow mask.

Figure 4: QA layer 3 (cloud and cloud shadow mask) and input PS-TOAR product exemplified for the AOI used in Figure 3.



A pixel traceability/provenance mask is also provided ([Figure 5](#)). This raster layer identifies the footprints of the PlanetScope scenes used to produce any given tile image (cloudy or clear). Each domain is associated with a unique integer value that is linked to a scene identifier (i.e., Itemtype/sceneID) embedded as metadata in the QA geotiff. The scene identifier (e.g., PSScene/20190701\_172222\_104e) provides the information needed to locate and access the source data through Planet’s API. The embedded metadata may be displayed using GDAL (e.g. `gdalinfo name_of_file.tif`). Note that the scene identifier is formatted as `<acquisition_date>_<acquisition_time>_<acquisition time seconds hundredths>_<satellite_id>`. This provides information on the time of acquisition for each pixel in the image.

Figure 5: QA layer 4 (pixel traceability mask) for the tile in Figure 3 (8000 x 8000 pixels) on July 1, 2019. In this case, a total of 10 PS ortho scenes from three separate strips were used to construct the tile image. The associated scene identifiers were extracted from the PF-QA embedded metadata. The visible seam lines in the PS-TOAR product result from merging Dove-R (reddish strip) and Dove-C (greenish strip) scene data with quite different spectral bands and Relative Spectral Response (RSR). Note that these transitions are not visible in the final PF-SR output.



QA layer 5 ([Table 5](#)) identifies the number of FLS-SR scenes (i.e., Sentinel-2 or Landsat 8/9) used for each pixel during reference sampling and calibration. In general the larger the number of reference scenes, the more robust the calibration is expected to be (see [Section 4.4](#)).

QA layers 6 - 9 provide band-specific confidence information for the “synthetic” (i.e., gap-filled) pixel values (a fixed 3% uncertainty is used for observed data). The process for deriving these is described in [Section 4.8](#). The confidence information is reported as an absolute percentage to indicate the deviation of the synthetic value from an actual observation. Accordingly, the absolute uncertainty in reflectance units can be calculated by multiplying the provided confidence information (x 0.01) with the corresponding surface reflectances recorded in the PF-SR product ([Table 3](#)).

### 3.3. SPATIOTEMPORAL ASSET CATALOG (STAC)

All Planet Fusion products are delivered with a SpatioTemporal Asset Catalog (STAC) file that conforms to the [STAC specifications](#). This STAC item contains information that summarizes the properties of the SR and QA

products. This includes the version of Planet Fusion that the products were generated with, the dates that the products were created, and support for several STAC extensions.

STAC Extension	Description
<a href="#">Electro-Optical</a>	Specification of the spectral bands contained with the SR product and descriptions of the information bands contained within the QA product
<a href="#">Projection</a>	Coordinates representing the bounding geometry of the tile's footprint
<a href="#">Raster</a>	Properties of the tile pixels

A STAC catalog is produced alongside all STAC items that contains an organizational structure to browse the STAC items. These STAC items and the static STAC catalog are delivered alongside the SR and QA products. A new STAC catalog with links to all new STAC items is delivered every time Planet Fusion products are delivered and overwrites any previously delivered STAC catalogs.

### 3.4. PROJECTION, GRIDDING, FILE NAMING, AND DELIVERY

Planet Fusion products are generated as regularly gridded raster tiles. Tiles have a 3 m pixel size, a 24 by 24 km extent (8000 pixel width and height), and are projected in the UTM zone intersected by their extent using the WGS-84 horizontal datum. Tile identifiers are based on a "{i}E-{j}N" template, where "i" is the zero-based easting index and "j" is the zero-based northing index using the origin of the UTM zone's coordinate reference system.

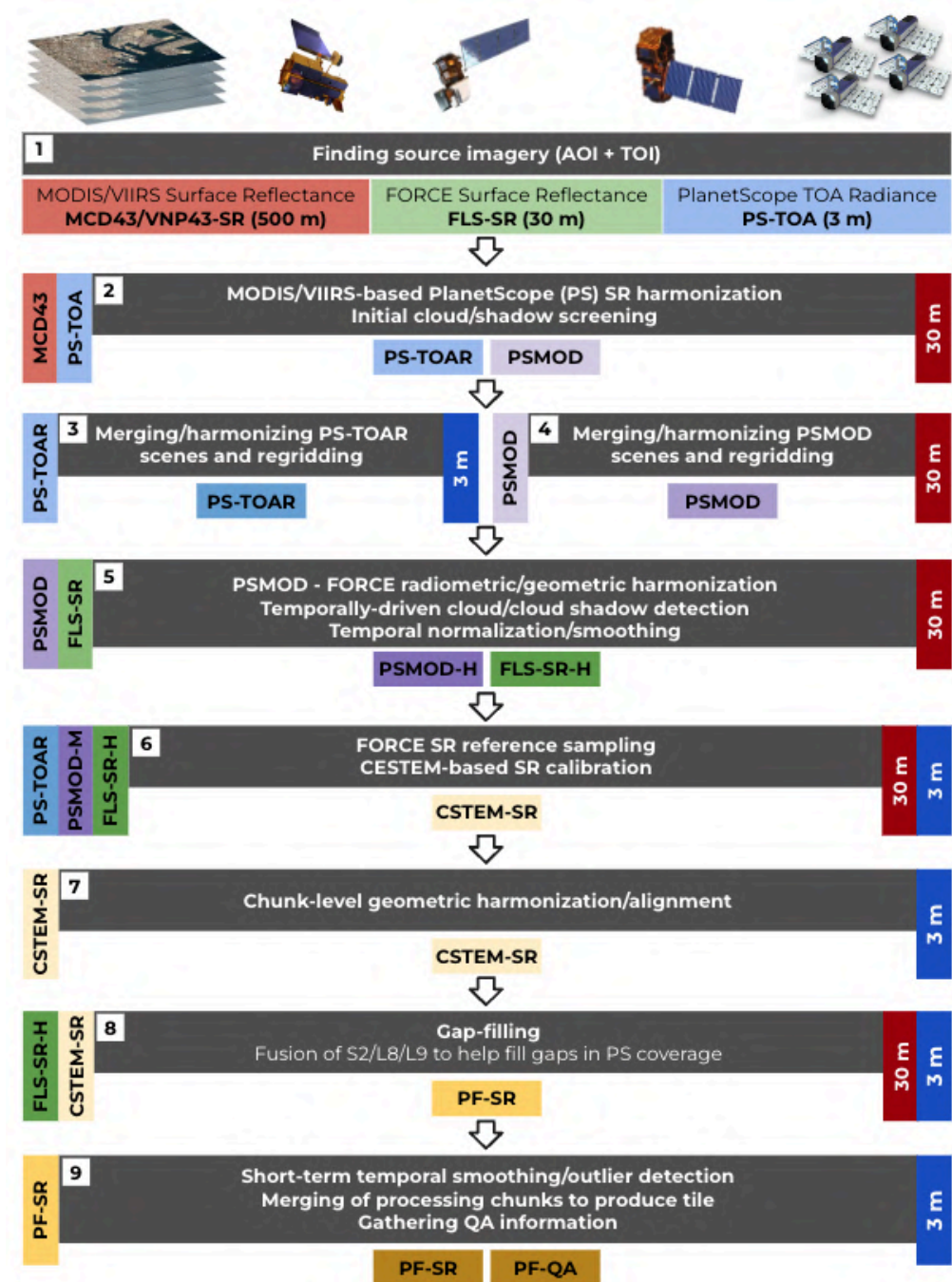
Tile Property	Description
Tile Size	24 km (8000 lines) by 24 km (8000 columns). Storage size varies with LZW compression. A typical Surface Reflectance tile consumes 300 MB. A typical Quality Assurance product consumes 5 to 15 MB.
Pixel Size	3 m
Spatial Reference	WGS-84 UTM zones based on tile intersection
Identifier	{i}E-{j}N Using coordinate system origin, i is the zero-based easting index, and j is the zero-based northing index.

The naming of the generated output files depends on the delivery mechanism. In general, file names are composed of the tile identifier, the product key, and the date. See [Table 2](#) for a description of each of the product keys.

For Google Cloud Storage delivery, products will be in a folder structure like "{scheme}/{zone}/{tile-id}/{product-key}/{date}.tif". For example, a Surface Reflectance tile for January 2, 2018 would be named like UTM-24000/15N/17E-192N/PF-SR/2018-01-02.tif (where UTM-24000 refers to the 24 km tiling scheme, 15N is the zone intersected by the tile, and 17E-192N is the specific tile id).

## 4. PLANET FUSION METHODOLOGY

Figure 6: A generalized overview of Planet Fusion processing modules for any given Fusion tile and TOI. The diagram highlights the key intermediate and final product artifacts, the associated pixel resolution (3 or 30 m) and processing features (e.g., cloud masking, radiometric and geometric harmonization, gap-filling, time-series processing, temporal filtering).



The overall methodological elements of Planet Fusion surface reflectance processing are diagrammed in [Figure 6](#). Planet Fusion products are based on an implementation of the CubeSat-Enabled Spatio-Temporal

Enhancement Method (CESTEM), which has been described in detail in [Houborg and McCabe 2018a/2018b](#). Planet Fusion processing includes significant refinements and additional functionality related to geometric harmonization, cloud masking, gap-filling, and sensor data fusion. Key elements of the approach and processing specifics are outlined below.

#### 4.1. TILE (CHUNK)-LEVEL STACKING

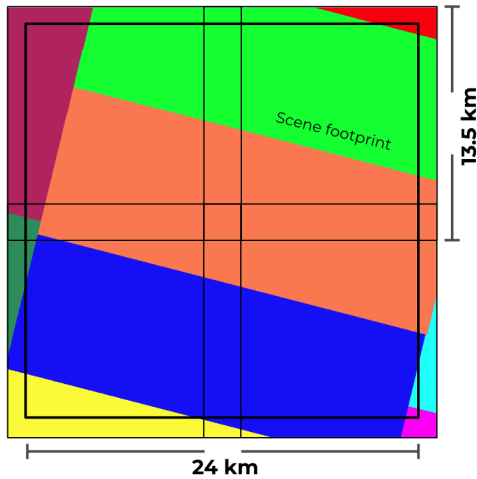


Figure 7: Visualization of a Planet Fusion tile with contributing PlanetScope scenes. Planet Fusion processing is done on slightly overlapping chunks (13.5 x 13.5 km) that are merged to produce the full tile (24 x 24 km).

After identifying the source imagery (PS-TOA, FLS-SR, PSMOD) that intersect with a given Planet Fusion tile over a specified Time Of Interest (TOI) (step 1, [Figure 6](#)), the respective input streams are stacked and re-gridded to the Planet Fusion tiling system ([Section 3.3, Figure 7](#)) with either a 3 m or 30 m pixel resolution (step 2/3/4, [Figure 6](#)).

In the case of the scene-based PlanetScope TOA reflectance (PS-TOAR) data, several scenes from multiple sensors may be overlapping with parts of the tile domain ([Figure 5, 7](#)). In order to retain the best data for the tile domain, priority is determined as a function of image quality category (prioritizing “standard” over “test” quality) (for more details on the image quality categorization see: [Roy et al., 2021](#)), initial cloud percentage (prioritizing scenes with the lowest cloud percentages), sun elevation (prioritizing scenes with the highest sun elevation), and scene overlap with the tile domain. The scene to tile conversion will also prioritize merging of scenes acquired from a single satellite in a single pass (i.e., strips) to reduce seam lines and spatial discontinuities introduced by cross-sensor inconsistencies. A phase correlation technique ([Section 4.5](#)) is used to help ensure that the PlanetScope scenes are geometrically aligned/co-registered (with sub-pixel precision) before compositing the tile. In addition, the re-aligned PS-TOAR scenes are brightness harmonized across the tile domain to facilitate a seamless Surface Reflectance calibration ([Section 4.4](#)). The brightness harmonization utilizes the clear-sky overlap between scenes to derive band-specific regression coefficients that are used to normalize the reflectance magnitudes across the scenes.

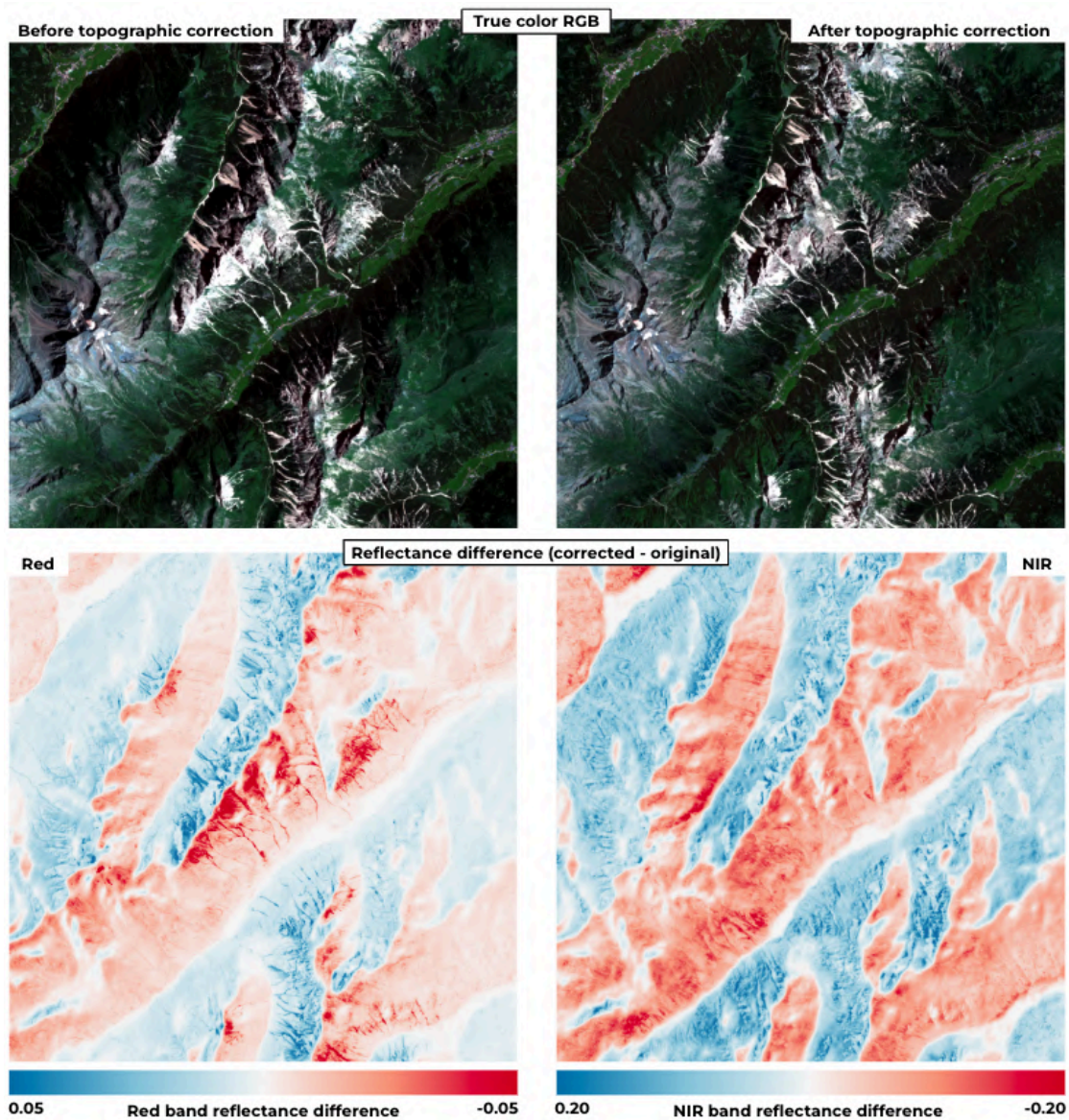
A 30 m resolution stack of MODIS/VIIRS Surface Reflectance-calibrated PlanetScope imagery (PSMOD) is also produced (step 2/4, [Figure 6](#)). The MODIS/VIIRS calibration is performed at the PlanetScope scene level using day-coincident MCD43/VNP43 NBAR products ([Table 1](#)) as the radiometric reference, translating PS-TOAR into MODIS/VIIRS-consistent SR data ([Houborg and McCabe 2018a, 2018b](#)) (step 2, [Figure 6](#)). The scenes are prioritized as described above for PS-TOAR when producing the tile. This also involves co-registration of the 30 m PSMOD scenes prior to merging and tile composition.

The FORCE-based Surface Reflectance tiles (FLS-SR) are mapped onto the Fusion tiling grid in a similar way.

Planet Fusion processing is done on slightly overlapping (i.e., a buffer of 750 m) chunks with a 13.5 by 13.5 km extent ([Figure 7](#)). The tile products are generated by merging data from 4 chunks, utilizing a gradual weighting and harmonization approach across chunk overlap zones to avoid visible boundaries (seam lines) in the final outputs. If the subscription AOI involves neighboring Fusion tiles an inter-tile blending module is invoked to use the same methodology to ensure seamless inter-tile transitions.

## 4.2. TOPOGRAPHIC CORRECTION

Figure 8: Visualization of the impact of the topographic correction on PlanetScope imagery acquired over a mountainous region in Austria on 2022-07-19. The impacts are significant over the sloping terrain with reflectance corrections ranging from approximately  $\pm 0.05$  (red) and  $\pm 0.20$  (NIR) reflectance units.



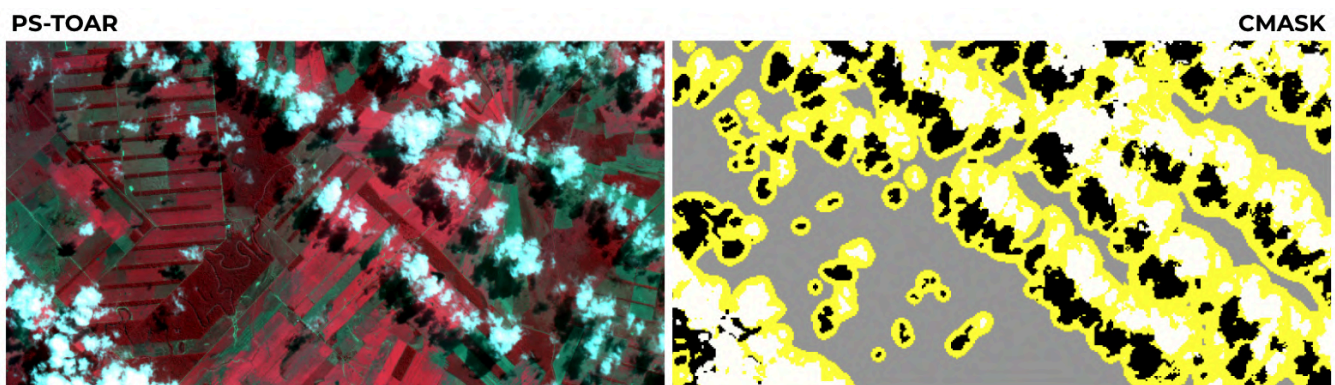
Topography (irregular shape of the terrain) will affect the surface reflectance as a function of sun illumination conditions (sun elevation and sun azimuth), terrain shape (slope and aspect), and surface and atmospheric characteristics. Topography can significantly alter the reflectance signal and obfuscate the interpretation of surface characteristics in space and time. Topographic corrections attempt to remove the effect of topography on reflectance so that identical surface phenomena (e.g., vegetation type) produce comparable reflectance signals irrespective of terrain characteristics.

The FORCE surface reflectance data have been corrected for the effects of topography on reflectance ([Frantz 2019a](#)). Starting with Fusion version 1.3.0 a topographic correction is also applied to the PlanetScope based product artifacts ([Figure 8](#)) produced by the Fusion pipeline. The adopted topographic correction shares similarities with the approach adopted in FORCE and is based on modeling illumination conditions using a Digital Elevation Model (Intermap World 30, <https://www.intermap.com/nextmap>) to compute slope and aspect information (using the GDAL “gdaldem” functionality) along with sun elevation and sun azimuth information from the PS scenes. For simplicity, Lambertian (i.e., no directional dependence on reflected light) surface conditions are assumed. The implementation is based on the Sun-Canopy-Sensor with C-correction approach described in [Soenen et al. 2005](#). The semi-empirical C-correction component is included to avoid over-corrections by accounting for the effects of diffuse radiation ([Teillet et al. 1982](#)). The topographic correction is applied to both PSMOD and PS-TOAR stacked product artifacts produced in step 3 and 4 ([Figure 6](#)). Applying the topographic correction to PS data is shown to significantly improve the agreement with day-coincident FORCE over AOIs with complex terrain ([Section 5.1](#)) and is expected to improve the overall quality of the Fusion data in regions with significant topography.

### 4.3. CLOUD AND CLOUD SHADOW MASKING

Planet Fusion cloud and cloud shadow detection (step 5, [Figure 6](#)) is performed at 30 m resolution using a temporally-driven approach that takes advantage of PlanetScope and FORCE (L8/9, S-2) surface reflectance information in a synergistic way. The approach is iterative and initialized with the original scene-based cloud and cloud shadow masks associated with both the PlanetScope and FORCE data. For PlanetScope, the initial cloud and cloud shadow mask is produced during the MODIS/VIIRS-based calibration stage (step 2, [Figure 6](#)) predominantly informed by UDM 2.0 (before 2023-11-23) or 2.1 (after 2023-11-23) detections, when available. A cloud verification approach is implemented at this step in an attempt to reduce commission/omissions errors.

Figure 9: Example of Planet Fusion cloud (white) and cloud shadow (black) detections over a region in Bolivia. Yellow represents the applied buffer around the detections.



The temporally-driven detection approach can accommodate PS and FORCE data acquired at different times on the same day. The multi-source input data are first geometrically harmonized (see [Section 4.5](#)) to improve detection results and reduce commission issues resulting from pixels not being properly aligned. The detection approach utilizes clear-sky observations (i.e., as identified by the initial cloud masks during the first iteration) over a flexible temporal window (up to  $\pm 1$  year) for any given 30 m pixel to help flag spectral outliers potentially resulting from cloud, cloud shadow, or haze contamination. The deep temporal stack of clear-sky observations is used to create a clear-sky background image for each acquisition date over the defined TOI. The clear-sky background image generation utilizes clear-sky information acquired from multiple dates in the past and future (if available) relative to the prediction date, and adopts daily class-specific spectral trajectories (derived on the

basis of the clear-sky imagery stack) to change adjust the past/future acquisition data to be more representative of surface conditions on the prediction date. After outlier screening, the temporally interpolated clear-sky observations are compared against the prediction date imagery to flag pixel domains (if any) exhibiting spectrally anomalous behavior (i.e., dips or spikes). A carefully weighted average of the multi-temporal clear-sky inputs (this will include the prediction date data if not identified as anomalous) are then used to create the clear-sky background image. Next, the clear-sky background image is used in combination with the actual image acquired on the prediction date to identify spectrally distinct classes using an unsupervised K-means clustering approach. A suite of spectral difference metrics, such as the difference in red and NIR reflectance between the background and actual imagery, combined with a set of carefully defined spectral thresholds and a number of other constraints are then used to classify each cluster as clear, cloud, cloud shadow, or haze. Additional cross-correlation tests between the background and actual imagery serve to further resolve and label any cloud, cloud shadow, and haze contaminations. Furthermore, a series of automated techniques are implemented to verify these classifications and avoid (to the extent possible) masking out actual change. This includes the integration of hillshade information to help reduce commission issues in landscapes with significant terrain shadowing.

The cloud detected areas are expanded using a buffer zone (i.e., adjacent cloud domain, layer 5 in [Table 5](#)) (see also [Figure 9](#)) to ensure that most of the contaminated pixels are removed from the final outputs. The outlined processing is repeated once to take advantage of the updated cloud mask in the construction of the clear-sky background images, which serve as critical inputs to reliably classifying cloud and cloud shadow clusters in the acquired imagery on any given day. The scheme will refine and update the scene-based cloud masks (30 m) associated with both the PS (PSMOD-H) and FORCE (FLS-SR-H) data (step 5, [Figure 6](#)).

After the completion of the iterative cloud masking step, a cloud verification step is invoked to further reduce commission errors. This step will only serve to unmask presumably false cloud/cloud shadow detections based on comparisons against updated clear-sky spectral trajectory signatures along with other verification metrics.

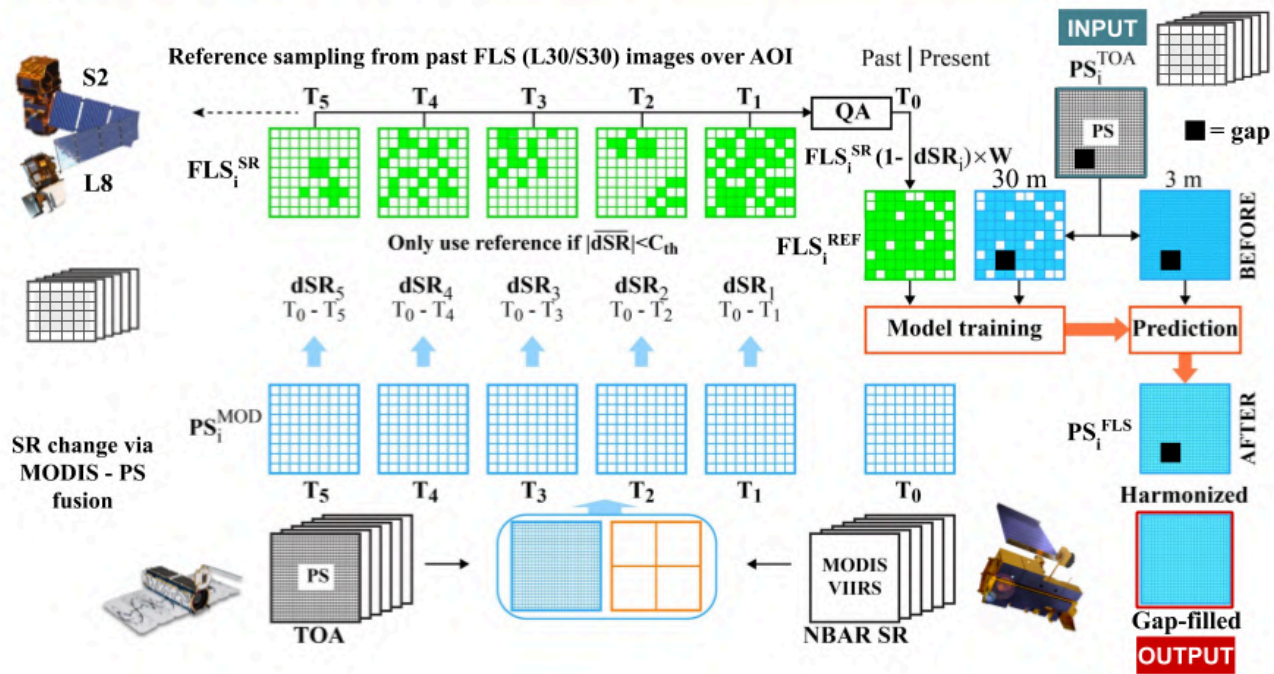
The cloud masking performance is evaluated in the Quality Monitoring section ([Section 5.3](#)).

#### 4.4. REFERENCE SAMPLING AND RADIOMETRIC HARMONIZATION

As its core, the Cubesat-Enabled Spatio-Temporal Enhancement Method (CESTEM) serves as a flexible mechanism to radiometrically harmonize multi-sensor spectral data into a consistent radiometric surface reflectance standard (i.e., the “gold standard” ). The FORCE-based surface reflectance product (30 m) ([Table 1](#); FLS-SR) is currently adopted as the gold standard. CESTEM is characterized by a number of unique features:

- Does not require day co-incident acquisitions (PS versus L8/L9/S-2) for cross-calibration/harmonization
- Implements a secondary MODIS/VIIRS-based harmonization to correct for surface reflectance changes occurring over given PS and L8/L9/S-2 acquisition time spans
- Effectively minimizes uncertainties associated with both PS and L8/L9/S-2 data via temporally-driven anomaly detection
- Can harmonize data from sensors with contrasting spectral bands and Relative Spectral Responses
- Is largely insensitive to noise (e.g., calibration uncertainties) in the input data (e.g., PS-TOA)
- Does not require PS inputs to be atmospherically corrected and is agnostic to PS input type (i.e., should work equally well with either DNs, TOA radiances, or TOA reflectances)
- The calibration model is locally constrained (i.e., specific to each PS chunk-level image domain) and therefore much less prone to overfitting and portability issues (e.g., “hallucinations”) relative to more generic AI driven model implementations

Figure 10: Diagram of the CESTEM radiometric harmonization framework, translating image stacks of PlanetScope TOA radiance ( $PS^{TOA}$ ) into FORCE-consistent Landsat 8/9/Sentinel-2 Surface Reflectance ( $PS^{FLS}$ ).



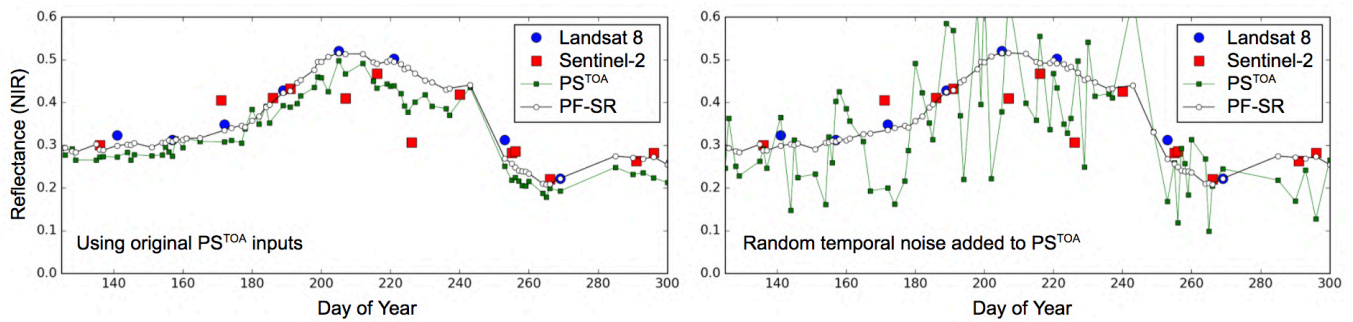
The CESTEM-based harmonization (step 6 [Figure 6](#), [Figure 10](#)) is applied to all images acquired over a defined Time Of Interest (TOI) drawing spectral (i.e., blue, green, red, and NIR) reference data from a pool of FORCE L8/L9/S-2 SR (FLS-SR) images acquired over a predefined “calibration window” (typically two years centered around the TOI). In order to reliably use past or “future” FLS-SR images for calibration purposes they must be associated with a day-coincident PS acquisition. Critical to this process is the use of MODIS/VIIRS-consistent (i.e., MCD43/VNP43) PlanetScope data ( $PS^{MOD}$ ) to quantify relative surface reflectance changes over given PS - FLS acquisition time spans ([Figure 10](#)). It follows that data from multiple FLS acquisitions will be sampled to generate a given PS coincident calibration reference image ( $FLS^{REF}$ ), using weights derived as a function of PS - FLS acquisition time spans and the magnitude of surface reflectance change relative to the prediction day ([Figure 10](#)). In addition, the multi-temporal FLS inputs are quality assured (QA) during the sampling step and outliers removed. Importantly, the calibration scheme can handle significant lags between the PS imagery to be harmonized and suitable FLS images as the calibration references can be sampled from images in the past or future (relative to the prediction date). As a result, the harmonization approach will continue to perform well over extended periods of cloudiness and FLS unavailability as long as a sufficient number of good FLS scenes can be identified within the “calibration window”. The associated layer 5 metadata ([Table 5](#)) will keep a pixel-specific record of the number of reference scenes available on any given day.

The multi-sensor and multi-time sampling approach ([Figure 10](#)) effectively minimizes potential issues and uncertainties (e.g., atmospheric contamination, cloud masking, BRDF effects, calibration inaccuracies) associated with both the PS and FLS data to create a very robust and temporally consistent radiometric reference. With this in place, a multivariate linear regression and decision tree approach ([Houborg and McCabe 2018a](#)) is employed to learn non-linear scene, sensor, and band-specific translational associations. The resulting models are then used to convert PS TOA ( $PS^{TOA}$ ) reflectances into FLS-consistent SR ( $PS^{FLS}$ ). During this process,

a number of techniques are implemented to avoid overfitting and to preserve band-specific textural features and spatial gradients present in the original 3 m PS imagery.

The CESTEM-based radiometric harmonization framework has been designed to be highly self-contained with “on-the-fly” radiometric correction models adapted to the characteristics of a specific sensor and local (chunk-level) surface and atmospheric conditions on any given prediction date. As such the framework is designed to effectively and accurately create sensor agnostic analysis ready data from distributed (virtual) sensor constellations. The framework is largely insensitive to temporal inconsistencies (“noise”) associated with the input data (PS<sup>TOA</sup>), which may result from calibration uncertainties and cross-sensor spectral differences. In fact, as showcased in [Figure 11](#), adding significant random temporal noise to the PS input data has a largely indistinguishable impact on the harmonized results. Another noteworthy feature is the low sensitivity to inaccuracies associated with the reference data, in this case mostly resulting from cloud omission errors in the FORCE-based Sentinel-2 data ([Figure 11](#)).

Figure 11: Illustration of the robustness of the CESTEM radiometric harmonization to noise in the input data streams (FLS and PS)



## 4.5. GEOMETRIC HARMONIZATION

The input imagery that feeds into Planet Fusion (e.g., L8/9, S-2, PS) has been orthorectified using rigorous preprocessing protocols with a positional accuracy typically better than 10 m RMSE. Nevertheless, perfect image to image alignment is difficult to achieve, particularly when combining data from disparate sensor sources. As Planet Fusion relies heavily on taking advantage of temporal information content for cloud masking, calibration, gap-filling, and smoothing, precise co-registration and sub-pixel fine alignment of stacked imagery becomes a necessity.

Planet Fusion uses an implementation of the phase cross correlation technique ([Guizar-Sicairos et al., 2008](#)) to robustly detect the global shift between two images with sub-pixel precision at various processing stages. Geometric harmonization/co-registration is applied to 1) PS scenes during the scene to chunk/tile conversion step (step 3/4, [Figure 6](#)), 2) PSMOD and FLS-SR imagery stacks (step 5, [Figure 6](#)), and 3) the CESTEM calibrated (CESTEM-SR) imagery stack (step 7, [Figure 6](#)), as described in more detail below.

Sub-pixel shifts (y, x) are derived based on the overlapping clear-sky domain between a source (to be shifted) and reference/anchor image on a per-band basis. The shifts are evaluated independently in multiple image subsets distributed within the clear-sky overlap region of the two images. An optimal set of image subsets are defined by optimizing the clear-sky data percentages (as close to 100% as possible) and the band-specific cross-correlation. The cross-correlation constraint serves to identify subsets with good alignment features and to reduce the impact of any residual contamination. It follows that the number and sizes of the subsets may vary significantly as a function of the clear-sky percentage of the images. Images with significant cloud cover

will typically be characterized by smaller subsets to fit within the clear-sky pixel "pockets". As the subsets must be completely gap-free to enable sub-pixel precision in the shifting estimates, the subset domain will be down-adjusted iteratively until that is achieved or the minimum domain size is reached. In the latter case, small remaining gaps will be filled via nearest neighbor interpolation to not lose the sub-pixel precision. If gaps still remain, shifts will not be derived for the given subset. The "global" (i.e., chunk-level) shift estimate will be based on an average of the subset-level shift estimates after outlier removal. If the derived shifts are within acceptable limits they will be applied to the source image using a Fourier transformation approach. Final acceptance of the shifted image will depend on a series of cross-correlation checks to verify that the spatial correlations between the source and reference image actually improved as a result of the pixel shift adjustments. Non-passing cross-correlation checks may indicate challenges associated with deriving a robust shift estimate due to image quality issues and/or scene registration issues leading to non-global shifts at the chunk-level. While the shifts are derived on a per-band basis, the final shift estimate will be based on the average of each band-specific shift given the generally high accuracy (~0.25 pixels for SuperDove) of the PlanetScope band-to-band alignment ([Planet Team 2023](#)).

Geometric harmonization is needed when creating the chunk-level image as it will typically combine scenes from multiple PlanetScope sensors ([Figure 5](#)), which may sometimes be slightly mis-aligned. The clear-sky overlap within a strip or between strips (i.e., a strip signifies the set of scenes acquired from a single satellite in a single pass) is used to assess the sub-pixel shifts as described above. If the shifts are deemed valid they will be applied (using the Fourier transformation approach) to ensure that the PlanetScope scenes within the chunk are geometrically harmonized (aligned) before merging. However, it will not correct for mis-alignments within the scene due to registration issues when creating the scene composite from raw frames (done upstream of Planet Fusion processing). This approach is applied to both PS-TOAR and PSMOD product artifacts during chunk-level stacking ([Figure 6](#)).

The 30 m stacked PSMOD and FLS-SR product artifacts are bundle-adjusted using a series of "moving" geometric reference images. The reference images are generated by averaging predominantly clear-sky high quality PSMOD images acquired within partly overlapping moving time periods distributed across the full processing TOI. A minimum number (ie., 10) of contributing PSMOD images will be enforced for this purpose to ensure robust and completely gap-free reference images. The contributing time window may be expanded to ensure enough candidate images are available. Subsequently, each stacked PSMOD and FLS-SR image is aligned against the closest reference image using the sub-pixel shift derivation approach outlined above.

The CESTEM calibrated (CESTEM-SR) imagery stack (3 m) is bundle-adjusted in a similar manner. In this case, the dynamic ("moving") geometric reference images will be generated by blending/averaging 8 multi-temporal candidate (e.g., clear-sky, high quality) CSTEM-SR images acquired over partly overlapping moving time periods across the full processing TOI. Pixel-level outliers will be flagged and removed before generating the geometric reference images. Then each individual CSTEM-SR image is aligned against the closest reference image as described above.

The geometric performance is assessed in the Quality Monitoring section ([Section 5.2](#)).

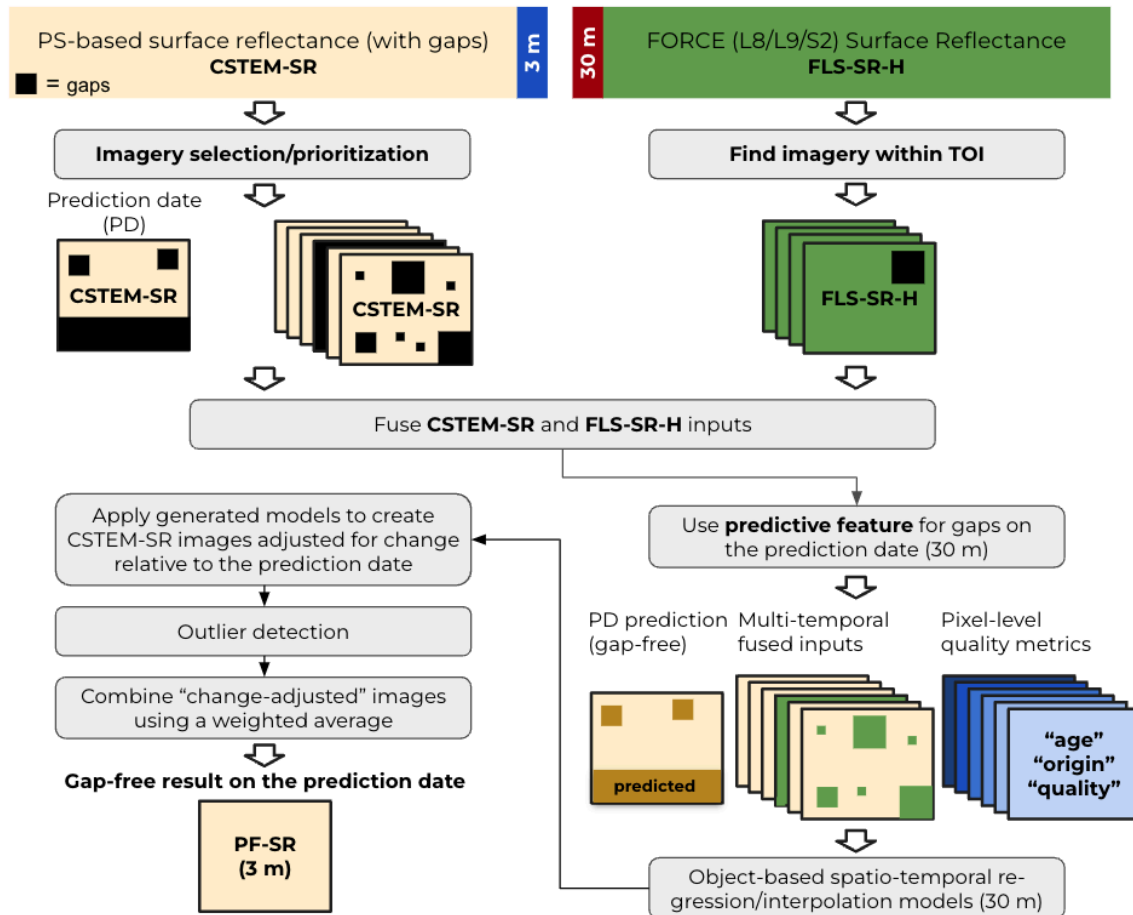
## 4.6. GAP-FILLING

The Planet Fusion gap-filling ensures a spatially complete and temporally continuous (daily) 3 m product irrespective of the actual acquisition coverage and cloud conditions. As this involves generation of estimated (synthetic) radiometric data, users are advised to utilize the associated QA metrics ([Table 5](#)) as measures of the synthetic data retrieval confidence. In general, the longer the daily interval gap is to the actual observation data (QA layer 2) the larger the overall uncertainty is in the gap-filled pixel values. Several other factors, such as surface characteristics, crop type, and vegetation dynamics are also thought to play an important role in

shaping the uncertainty associated with gap-filled Planet Fusion data values. These interacting factors will be reflected by the derived confidence estimates to some extent ([Table 5](#) and [Section 4.8](#)).

The gap-filling subprocess ([Figure 12](#)) is informed by cloud masked, radiometrically calibrated, topographically corrected, and geometrically aligned SR data (CSTEM-SR) in combination with complementary FORCE (30 m) L8/L9/S-2 data (FLS-SR-H) available within a temporal buffer centered on the prediction date.

Figure 12: Flowchart of 3 m (left side) and 30 m (right side) processing elements in the PF gap-filling module.

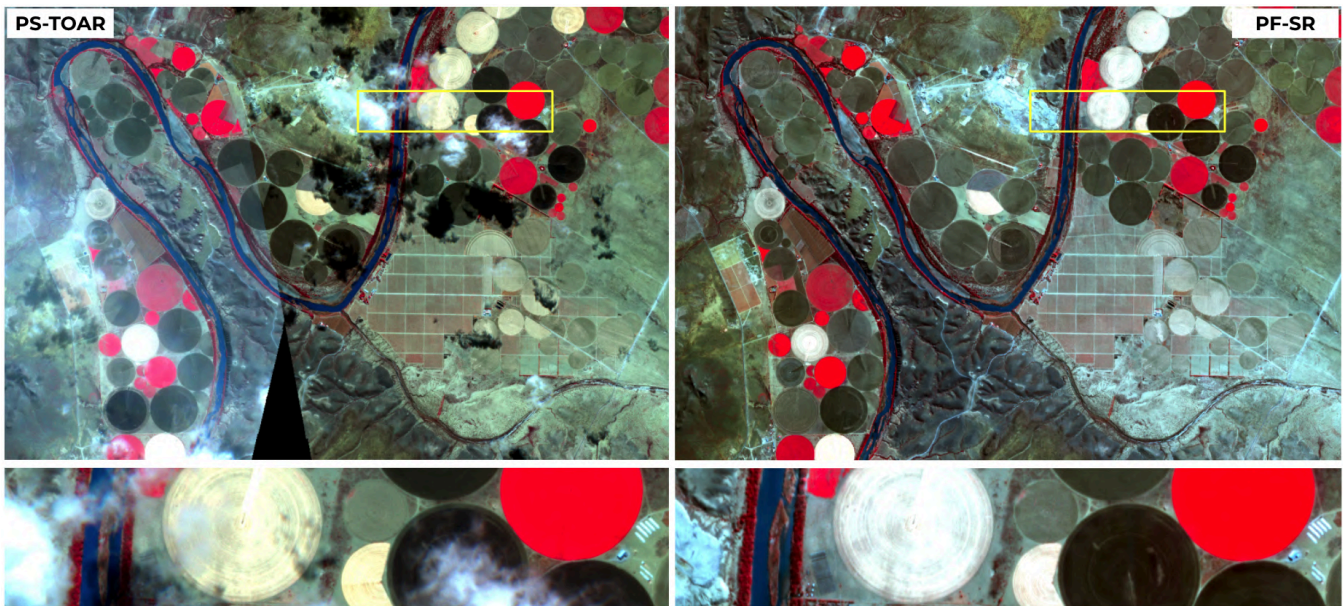


The chunk-level images (CSTEM-SR) used to inform the gap-filling process may originate from both before and after (if available) the prediction date, and are selected as a function of image quality category (prioritizing “standard” over “test” quality), cloud percentage (prioritizing scenes with the lowest cloud percentages), and time lag relative to the prediction date (prioritizing images acquired with the shortest lag). The gap-filling reference images are selected at the tile level to ensure consistency among predictions for chunks within a tile. The selected multi-temporal input images undergo a series of anomaly-based quality checks to flag (and mask out) pixel-level outliers resulting from residual cloud contamination or other image quality issues.

The CSTEM-SR images will then be resampled to 30 m to help build object-based spatio-temporal interpolation models that will be used to adjust the 3 m CSTEM-SR images for reflectance change relative to the prediction date. FLS-SR-H images (30 m) acquired within a temporal buffer of the prediction date will also be used to inform the interpolation and help fill observation gaps in the resampled CSTEM-SR images, if possible. The pixel domains in the vicinity of any remaining gaps will be filled using a class-specific nearest neighbor interpolation technique with confidences assigned as a function of the spatial proximity to an observed pixel value. The

objects (i.e., clusters) are defined on the basis of a temporally driven Kmeans clustering approach that uses principal components derived from a deep time series (~1 year) of harmonized surface reflectance images. The resulting clusters group pixels that are spectrally similar in space and time, and the object-based approach serves as an effective mechanism to learn surface reflectance dynamics over masked (i.e., cloudy) pixels using information from associated (i.e., from the same cluster) clear-sky pixels. To further aid/constrain the generation of the object-based interpolation models, a “predictive” feature ([Section 4.6.1](#)) is used to generate a complementary gap-free 30 m image to represent surface reflectance conditions on the prediction date ([Figure 12](#)). This predicted image is used in combination with the fused (CSTEM-SR + FLS-SR-H) inputs to derive band-specific object (cluster) based regression/interpolation models (first or second order) with regression fitting weights assigned as a function of a number of image-based metrics including the pixel “age” relative to the prediction date, the pixel “origin” (e.g., observed or nearest neighbor spatially interpolated), and the pixel “quality” ([Figure 12](#)). Object-level outliers will be removed during this process to ensure robust regression fits.

Figure 13: Impact of Planet Fusion cloud screening, gap-filling, and temporal filtering ([Section 4.7](#)) over a region around the Orange River in South Africa. It shows the original PS TOA reflectance data on the left and the resulting gap-free PF Surface Reflectance data on the right.



The resulting object-level regression/interpolation models serve as a way to incorporate both temporal and spatial information content to inform pixel-level gap-filling. They are applied to the selected 3 m CSTEM-SR images to adjust for predicted pixel-level surface reflectance change occurring between the CSTEM-SR acquisition dates and the prediction date while preserving the spatial 3 m texture in the CSTEM-SR images. Finally, the “change-adjusted” CSTEM-SR images are combined using a weighted seamless blending approach to fill gaps on the prediction date ([Figure 12](#)). The gap-fill confidence metric (QA layer 2, [Table 5](#)) will only record the number of days to the closest pixel-level observation used to gap-fill. As described above, data observed on other dates will also be used to inform the pixel-level gap-filling albeit with a rapidly decreasing weight as the number of days passed since the prediction date increases. The PF-QA product will provide full traceability into the source data used to fill the gaps, which includes tiff embedded metadata on the dates of all the images used to inform the gap-filling. [Figure 13](#) showcases the process from cloud contaminated PS-TOA reflectance to clean gap-free surface reflectance imagery using the outlined methodology.

#### 4.6.1. Predictive feature

A predictive feature has been implemented to improve gap-filling performance during more extended periods of cloudiness (or limited data availability) or when running Fusion in forward-fill (FF) mode ([Section 4.9](#)). In the latter case (i.e., FF), the predictive feature functions as a “forecaster” of surface reflectance on the prediction date based on surface reflectance trends learned from past data.

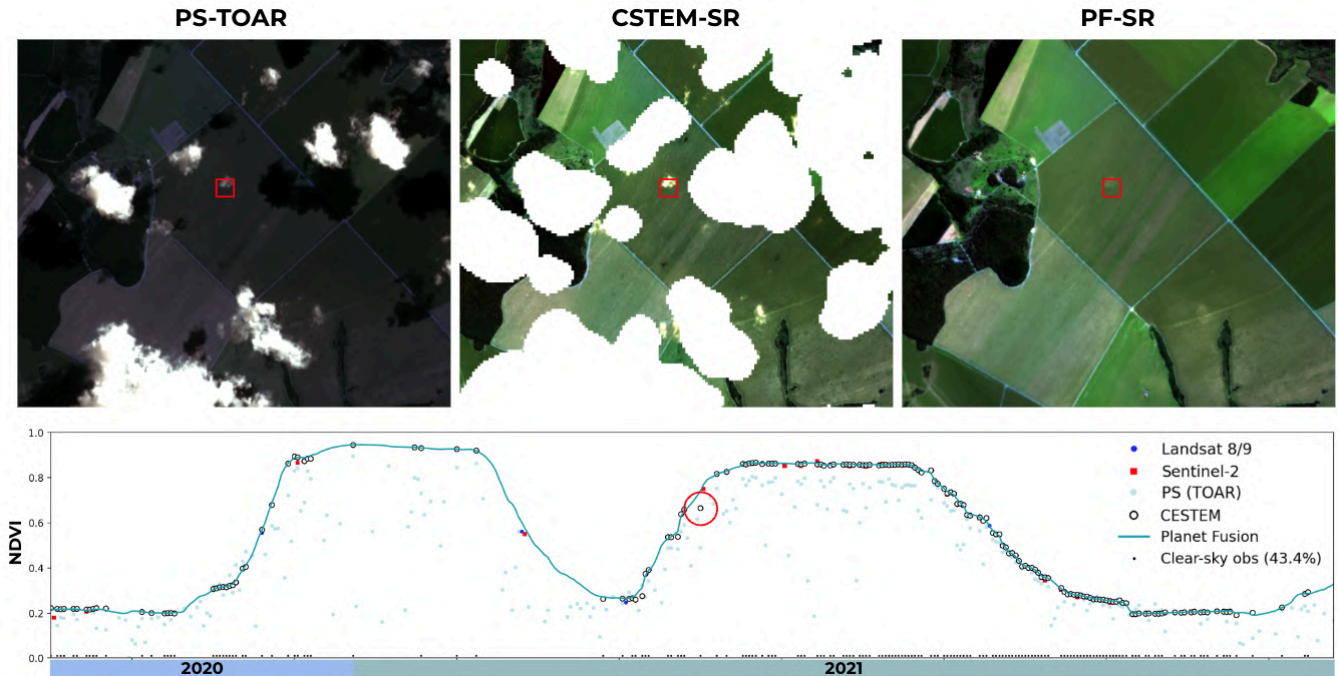
The predictive feature relies on object/cluster-level spectral signature trajectories derived from past imagery. In backfill mode (BF, [Section 4.9](#)) the spectral signature trajectories are derived on a yearly basis based on the cloud-masked CSTEM-SR product artifacts supplemented with complementary FORCE-based data (FLS-SR-H). As described above, a temporally driven Kmeans clustering approach is used to group spectrally distinct pixels (e.g., pixels with similar phenology), and spectral signature trajectories are derived for each cluster. The spectral trajectories hold information on band-specific surface reflectance change over time, which is used directly in BF mode along with the associated cluster map to predict a prediction date image to help constrain the object-based regression/interpolation models as previously described.

In FF mode we can take advantage of the final (gap-free) Planet Fusion product artifacts (PF-SR, [Figure 6](#)), generated in the associated BF run (i.e., BF data is a prerequisite for a FF run), to derive historic yearly cluster-based spectral signature trajectories for each year processed during the BF operation. In parallel cluster-based spectral trajectories representative of the most current clear-sky imagery will be generated based on an updated cluster map that prioritizes observations acquired within the last 2 months relative to the prediction date. It follows that an updated series of spectral trajectories will be generated for each prediction date during FF operation. The “current” trajectories will be based on clear-sky observations available since January 1 of the prediction date year up till the prediction date. In order to enable predictive “forecasting” we need to extend the “current” trajectories beyond the date of the last clear-sky observation, which may be several days before the FF prediction date (i.e., today) due to cloud cover. This is facilitated by fusing the “current” and “historic” spectral trajectories. We use dynamic time warping to find the optimal non-linear alignment (i.e., lowest spectral distance) between two time series. Each of the “current” trajectories is matched against the available “historic” trajectories over the overlap period and the best trajectory match is determined based on the lowest spectral distance derived from the dynamic time warping approach. During this process, various day-shifts will be applied to the “historic” trajectories to account for potential differences in the timing of phenological transitions (e.g., green-up) between years. In addition, data closest to the prediction date will be weighted the most in the spectral distance computation. Once a match has been identified, the “current” trajectories can be extended to the full year (into the future relative to the prediction date) using the information from the matched “historic” trajectories.

With the extended (full year) predictive trajectories in place, the 30 m prediction date image needed during gap-filling ([Figure 12](#)) can be “forecast” (i.e., extrapolated) from the past image information (CSTEM-SR). As this predictive process can be associated with a fair deal of uncertainty, various trajectory verification mechanisms are in place to reduce the risk of using trajectories that may poorly represent actual surface reflectance change trends. The predictive feature is a critical mechanism to guide the temporal interpolation when you have significant gaps in the clear-sky observation record around the prediction date, and is instrumental in ensuring robust gap-filling during FF operation.

## 4.7. TEMPORAL FILTERING

Figure 14: Planet Fusion temporal filtering in action over a region in Brazil. Small cloud elements are missed by the temporally-driven cloud detection on this date, and show up as dips in masked (CSTEM-SR) NDVI time series. The temporal filtering approach effectively detects these as anomalies to ensure a final product artifact (PF-SR) free of contamination.

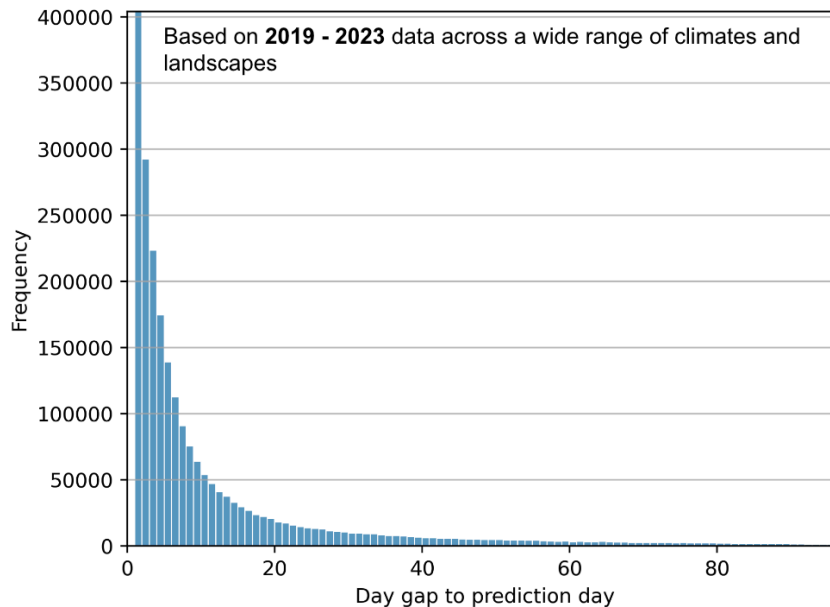


A conservative/cautious short-term temporal filtering algorithm is applied to the daily gap-free image stack in an attempt to correct for any remaining anomalous spectral behavior and produce highly clean and temporally consistent time series data (step 9, [Figure 6](#)). This algorithm will predominantly apply smoothing on pixels flagged as “anomalous” based on spectral comparisons with corresponding pixel retrievals originating from up to a 5 day window centered on the prediction date (i.e.,  $\pm 2$  days) with a minimum of 1 observation both before and after the prediction date. The smoothing weights are determined as a function of the magnitude of the spectral differences (i.e., spikiness) and spectral similarity between observations over the filtering window, and will take into account neighborhood information and spatial texture in order to avoid introducing spatial discontinuities/artifacts. The algorithm is very “cautious” and will only apply minor (if any) smoothing to the majority of pixels ([Figure 14](#)). Its key benefit lies in identifying and removing/reducing residual contamination (e.g., missed cloud/shadow/haze elements, image quality issues) in the images to produce a “clean” SR output that can be trusted to represent actual surface changes not confounded by atmospheric contamination. As the filtering relies on anomaly detection there’s a risk that it sometimes will smooth out actual change events. This particularly applies to very short-term change events such as moving ships (they may disappear) but may also apply to certain flooding events given significant clear-sky data sparsity. [Figure 14](#) exemplifies how the temporal filtering step helps identify residual cloud contamination in the intermediate CSTEM-SR product artifact. The highlighted missed cloud feature shows up as an NDVI anomaly in the associated time series plot and is assigned a minimal weight during temporal filtering to produce a final product artifact (PF-SR) without these contamination artifacts. This anomaly-based approach works particularly well alongside an effective cloud screening process with limited omission as that will increase the likelihood of successful anomaly detections. The NDVI time series ([Figure 14](#)) of the intermediate cloud masked product artifact (CSTEM-SR) suggest very effective cloud screening (see also [Section 5.3](#)), and the generally minor differences observed between CSTEM-SR and PF-SR ([Figure 14](#)) support the notion of a “cautious” temporal filtering algorithm.

## 4.8. CONFIDENCE INFORMATION

The QA file provides band-specific confidence information of the gap-filled (synthetic) surface reflectance estimates ([Table 5](#)). The band-specific confidence information is reported for each 3 m pixel as an absolute percentage, which can be used as an approximate assessment of the uncertainty of the estimate relative to a real surface reflectance observation.

Figure 15: Histogram showing the frequency of absolute day gaps (relative to the prediction date) in the multi-AOI training dataset used to generate the confidence models.

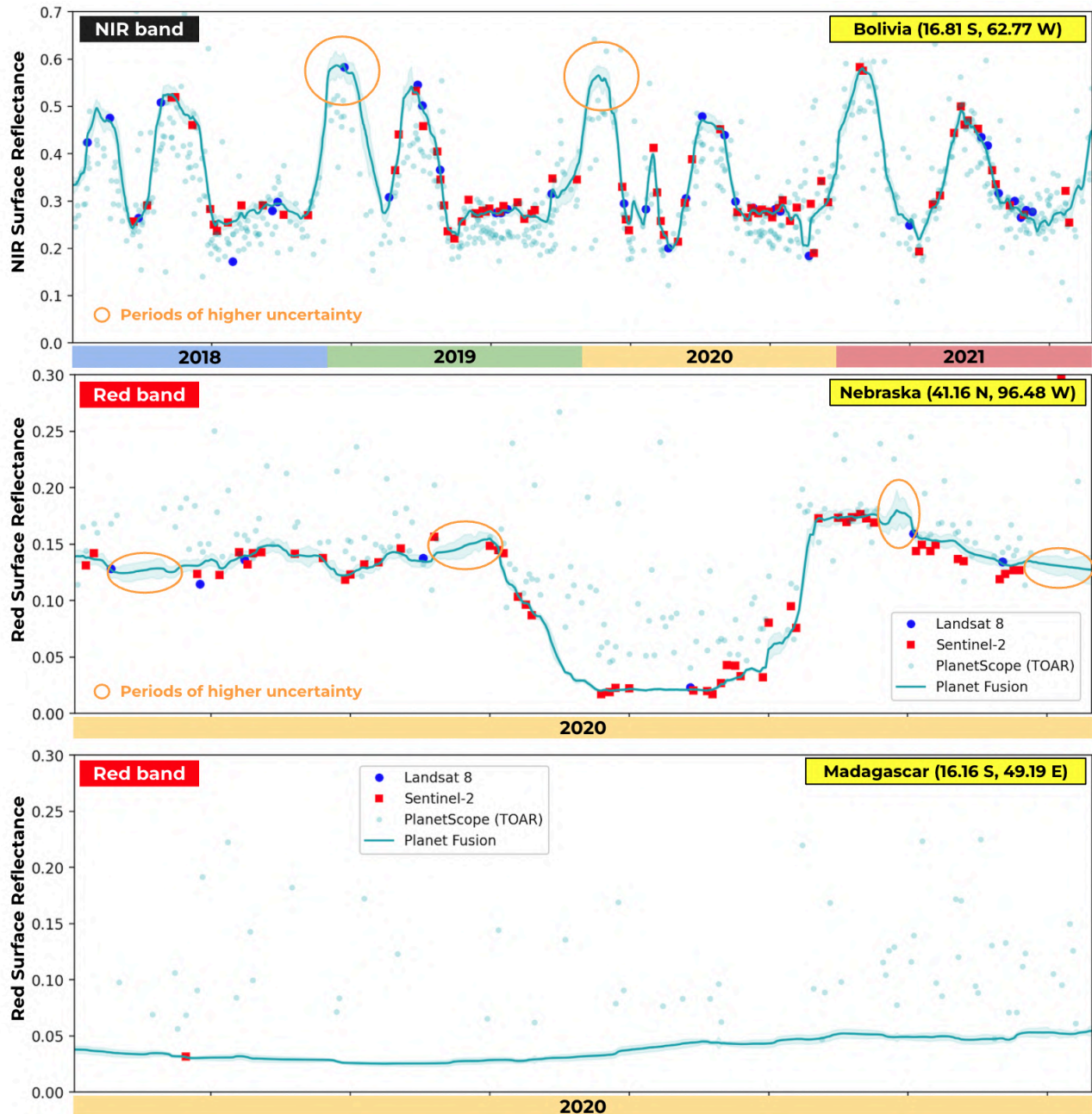


The models used to derive the band-specific confidence information are based on comparisons between observed and predicted/gap-filled SR data over a selection of representative AOIs ([Figure 19](#)) and TOIs covering a wide gradient in surface characteristics and cloud conditions ([Figure 15](#)). The training data are generated by running the gap-filling module ([Section 4.6](#)) with the clear-sky observation data on the prediction date removed. The absolute relative difference between the observed and predicted/gap-filled surface reflectance (for the same pixels) serves as the target variable (i.e., the uncertainty), which is related to a set of explanatory feature variables using a machine learning technique. The explanatory variables include 1) the 4-band spectral data, 2) NDVI, 3) the number of days to the closest observation used to gap-fill ([Figure 15](#)), and 4) a surface reflectance change metric. The “global” confidence models trained for each spectral band can then be applied to a given Planet Fusion tile considering a day and tile-specific explanatory input dataset.

[Figure 16](#) showcases the time series of derived confidence estimates over AOIs characterized by significantly different cloud conditions and cover types. Over agricultural fields in Bolivia (top panel) and Nebraska (middle panel) periods of higher predicted uncertainty generally coincide with more extended gaps in the PS observation record resulting from clouds or snow due to an expectedly tight coupling between SR uncertainties and the “age” (relative to the prediction date) of the pixels. However the red reflectance time series over a forested pixel in Madagascar has a relatively low associated uncertainty (bottom panel), despite the extreme cloud environment and significant pixel “ages” (e.g., only one clear-sky S-2 observation was available over the one year period). This seemingly contradictory information can be explained by cover type differences (from agriculture to forest). The spectral signature of an evergreen/tropical forest canopy is relatively stationary in time relative to the spectral signature of a crop canopy going through various development stages (e.g., planting, green-up, maturity, senescence, harvest), which will tend to make gap-filling over such forested pixels less uncertain even during extended periods of clouds. The explanatory surface reflectance change variable is

effective at capturing such subtleties during confidence model training. Still, synthetic pixel uncertainties are controlled by a complex interaction of several factors, and the provided confidence estimates should only be considered as a rough approximation with a fair degree of uncertainty at this time.

Figure 16: NIR and red band time series results over agricultural and forested AOIs in Bolivia (top), Nebraska (middle), and Madagascar (bottom) with associated confidence intervals (the colored area around the Planet Fusion solid line).



## 4.9. BACKFILL VERSUS FORWARD-FILL OPERATION

Planet Fusion can be run in either backfill or forward-fill mode. Backfill signifies a run over a time of interest in the past. A backfill run over at least a 2 year period is always initially required to establish deep temporal image stacks to inform the cloud masking, calibration, harmonization, and gap-filling processes. Forward-fill jobs are executed subsequent to a complete backfill operation and typically run as close to present time as possible and typically on a daily basis, processing any new imagery that has become available since the last job execution utilizing information from the deep temporal stacks generated during the backfill for cloud masking, calibration, and gap-filling purposes. Currently a 48 hour latency of delivering Planet Fusion tiles during daily forward-fill operation is targeted, which is a function of the latency of the input sources (i.e., primarily PlanetScope and MODIS/VIIRS) and processing time.

As described in [Section 4.6](#), gap-filling is notably different during backfill and forward-fill operation. While data is typically available both before and after a given prediction date in backfill operation, a forward-fill run is intrinsically constrained in the forward looking direction, which tends to increase the uncertainty of synthetic pixel retrievals (as you don't know what is "around the corner"). As described in [Section 4.6](#), a predictive/forecasting feature based on trends learned from historic observations is employed during gap-filling to make better informed predictions in forward-fill mode.

Other factors may cause differences in product quality between forward-fill and backfill operation. Forward-fill typically involves near real-time (NRT) data processing and the inherent latencies in satellite data and FORCE processing can cause S-2 and/or Landsat scenes acquired close to the prediction date to not be available to inform the calibration process. While the multi-temporal calibration approach should continue to perform well based on FORCE data acquired in the past relative to the prediction date, the inclusion of the most current (relative to the prediction date) information will tend to be beneficial. The temporally driven cloud detection approach will also benefit from having data available both before and after the prediction date to most effectively detect anomalies attributable to cloud, cloud shadow, or haze contamination. In daily forward-fill, the anomaly detection is based mostly on backwards looking imagery (i.e., only data from one day in the future of the prediction day will be available at most), which can increase the risk of commission or omission errors in the cloud mask. Finally, in forward-fill (or when running Planet Fusion within 9 days of present day) NRT MODIS or VIIRS surface reflectance products will be used over the standard products ([Section 2](#)). The NRT MODIS/VIIRS products rely on backwards looking data alone to inform the BRDF correction and may therefore be less representative of prediction date surface conditions. While a bias correction procedure has been implemented to remedy this potential issue, the generally lower quality NRT MODIS/VIIRS data may impact the quality of the MODIS/VIIRS-based surface reflectance harmonization ([Figure 6](#)), which in turn may impact the accuracy of the CESTEM-based radiometric harmonization.

## 4.10. PIXEL RESOLUTION DEPENDENT DATA FUSION OPTIONS

Table 6: Overview of data fusion configurations as a function of target pixel resolution.

Planet Fusion	Direct <sup>1</sup> data fusion			Indirect <sup>2</sup> data fusion (S-2 + Landsat)			
	Pixel size	PS	S-2	L8/9	Calibration	Cloud masking	Gap-filling
3 or 5 m	✓				✓	✓	✓
10 m	✓	✓			✓	✓	✓
30 m	✓	✓		✓	✓	✓	✓

<sup>1</sup> With direct data fusion, the listed sources will be directly reflected in the clear-sky "CESTEM-SR" product artifacts

<sup>2</sup> With "indirect" data fusion, the inputs will be used to inform calibration, cloud masking, and gap-filling

While the default pixel resolution is 3 m, Planet Fusion (PF) can be customized to also run with target pixel sizes of either 5, 10, or 30 m, which will have implications for how the multi-source data streams are featured and used (i.e., direct versus indirect data fusion) in the final product artifacts (Table 6). As described in the previous methodology sections, when running PF at 3 m (or 5 m) PlanetScope observations will be directly “inserted” in the clear-sky product artifacts whereas S-2 and L8/9 (reported at 30 m) will be used indirectly (i.e., indirect data fusion) for calibration, cloud masking, and gap-filling purposes. With a 10 m target pixel size, S-2 will be treated exactly as PlanetScope (i.e., direct data fusion) and directly “inserted” alongside the PS data. This also means that the input S-2 TOA reflectance data will undergo the same radiometric and geometric harmonization/correction as the PlanetScope TOA reflectance data to produce a sensor agnostic output. In this case, the QA layer 4 pixel traceability mask (Table 5) will provide insights into the specific sources (PS or S-2) used. In the 30 m configuration the PS and S-2 data will be complemented with any available Landsat 8/9 images via direct data fusion. At 30 m, we don’t start from TOA reflectance data but rather use the FORCE-processed S-2 and L8/9 SR data.

These data fusion scenarios can provide valuable insights into the contributions of individual satellite sensors or constellations to clear-sky observation statistics. The Planet Fusion NDVI time series depicted in Figure 17 was generated based on a 30 m target pixel resolution configuration (Table 6) with all sensor sources (PS, S-2, L8/L9) combined and processed similarly (i.e., direct data fusion). This data fusion scenario gives an overall clear-sky coverage (100% = daily coverage) of 64.5%, which translates to a clear-sky revisit frequency of 1.55 (1 = daily coverage). A breakdown into individual sensors/constellations reveals a reduction in the overall clear-sky coverage from 64.5 to 60.5% with the default 3 m Planet Fusion configuration (i.e., PlanetScope only), whereas using S-2 and Landsat alone amounts to a 17.4% clear-sky coverage. Despite the significant drop in clear-sky revisit frequency, the combined S-2 and Landsat record appears to capture the majority of the phenological dynamics over this predominantly clear-sky AOI in South Africa. The clear-sky observation statistics vary between years in response to changing satellite sensor configurations and cloud cover conditions. Contributions from the different PlanetScope generations are expectedly highly time dependent with full Dove-C dominance from 2017 - 2018/2019, an interim of Dove-R imaging from 2019 to 2021, and SuperDove imaging starting in 2020 before reaching full dominance in 2022 (Figure 17).

Figure 17: Top panel: Multi-source NDVI time series over a 7-year period for a crop field near the Orange River in South Africa. The Planet Fusion results are based on a 30 m target pixel resolution configuration (Table 6). Bottom panel: Breakdown of the contributions of various sensor source combinations (data fusion scenarios) to yearly and overall (all years) clear-sky coverage and revisit frequency values.

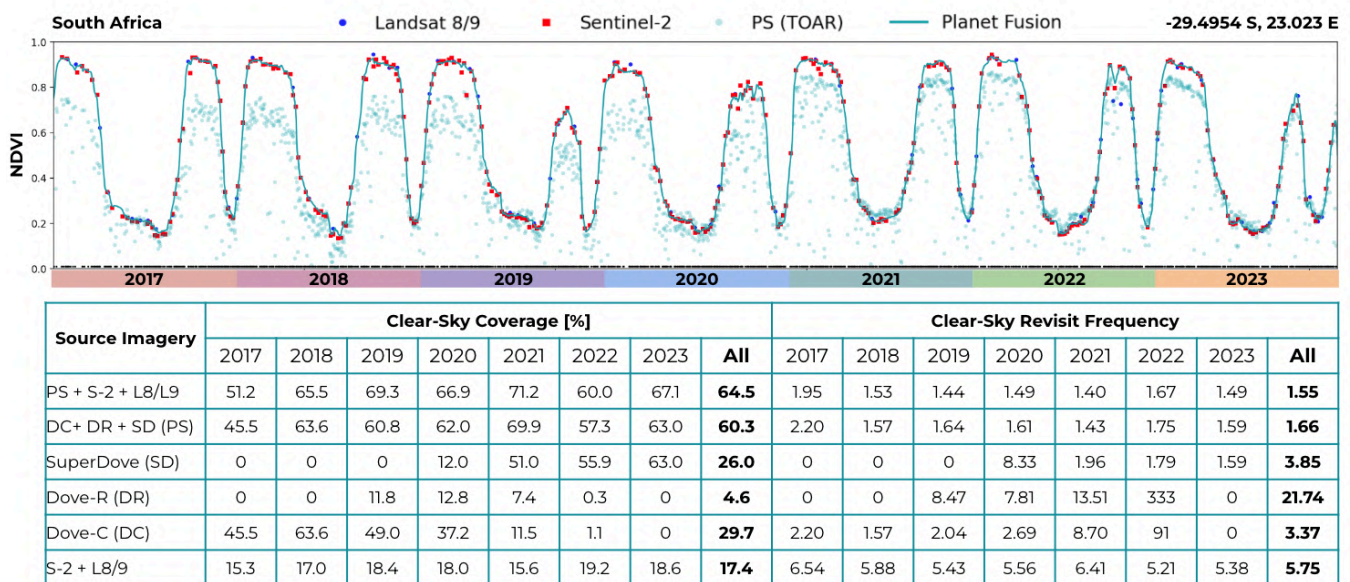


Figure 18: Top panel: Multi-source NDVI time series over a 7-year period for a crop field in the Goias region in Brazil. The Planet Fusion results are based on a 30 m target pixel resolution configuration (Table 6). Bottom panel: Breakdown of the contributions of various sensor source combinations (data fusion scenarios) to yearly and overall (all years) clear-sky coverage and revisit frequency values.

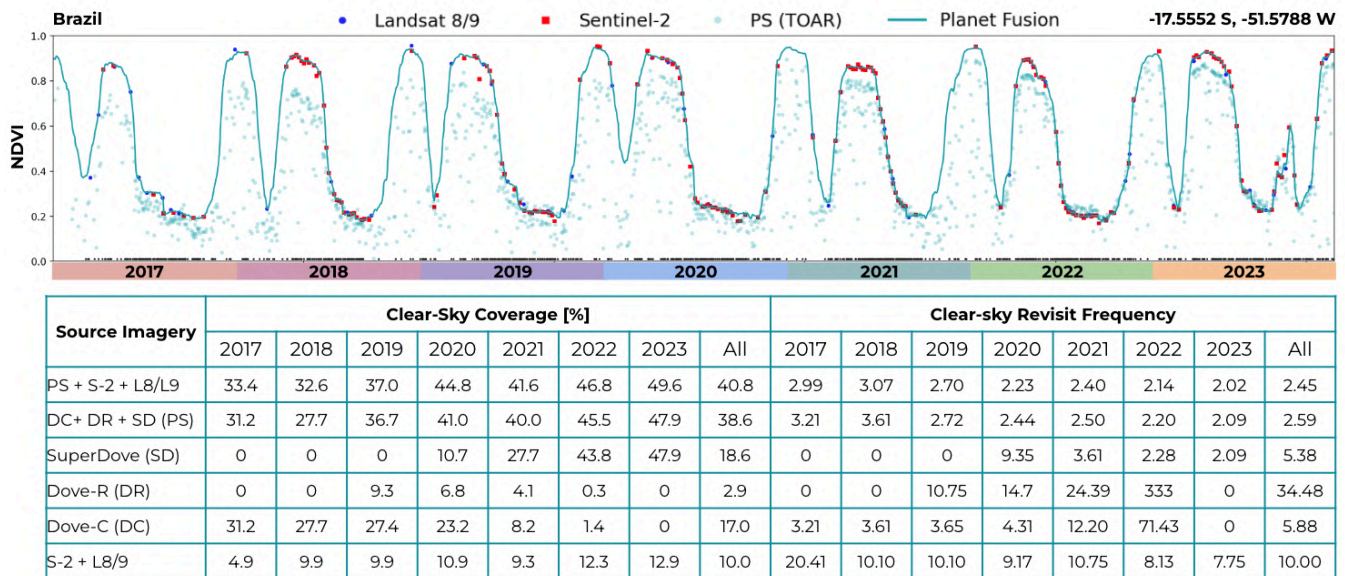
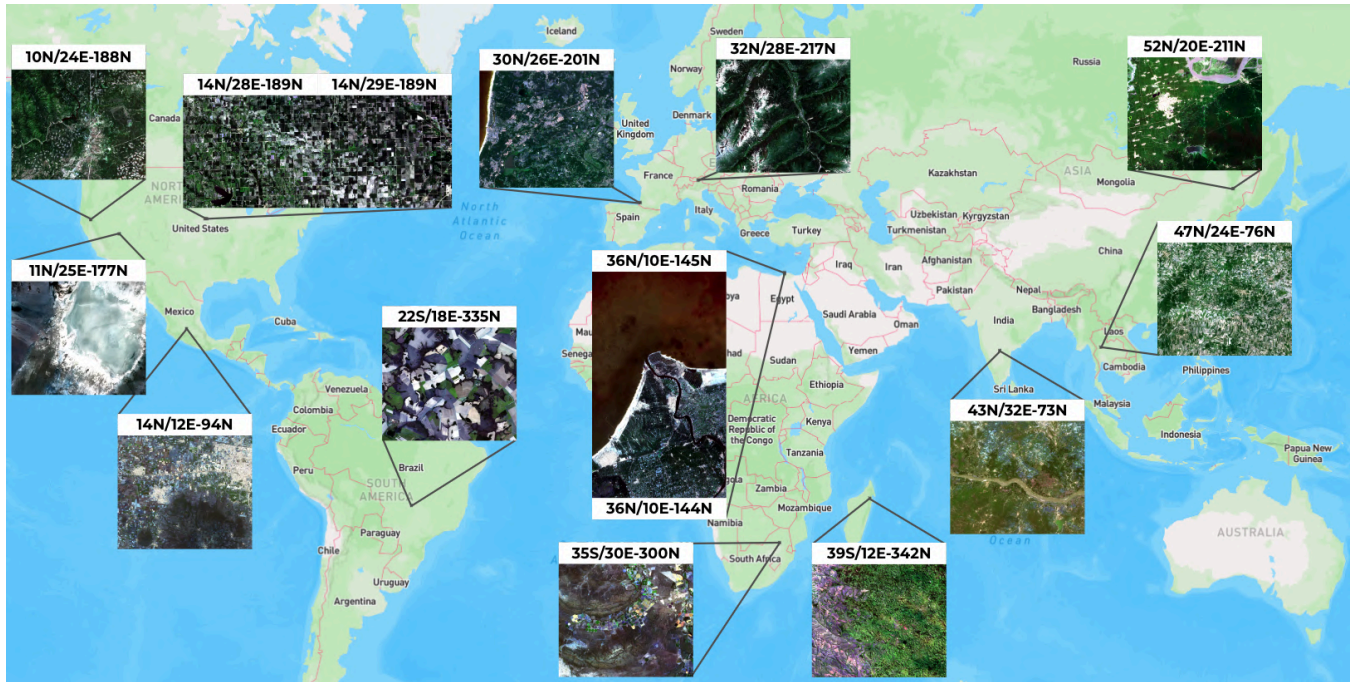


Figure 18 provides a comparable time series and clear-sky observation analysis over a more cloud prone region in Brazil characterized by extended periods of clouds. With public mission data alone (S-2 and Landsat) you get a clear-sky observation every 10 days on average but with significant inter-year and seasonal variations with occasional clear-sky observation gaps as high as 120 days (2020 to 2021 transition period). Noteworthy is the bump up in clear-sky coverage from 2022 and onwards, which may be related to the launch of Landsat 9. With the integration of PlanetScope the overall revisit frequency increases drastically from 10 (S-2 and Landsat) to 2.45 (all sources), which highlights the importance of integrating/fusing observations from multiple sensor sources to more effectively track land surface dynamics/phenology over regions such as this. Still, even with PlanetScope, significant gaps can be observed in the clear-sky record (as indicated by the black dots near the x-axis in Figure 18). While the Planet Fusion gap-filling technique appears relatively effective at restoring the phenological growth cycles during these data-limited periods, multi-modality (i.e., SAR - Optical) data fusion has the opportunity to provide uninterrupted insights on surface dynamics to help inform the gap-filling under extended periods of cloud cover. Work is currently underway to integrate “cloud penetrating” Synthetic Aperture Radar (SAR) data (Sentinel-1) into Planet Fusion.

## 5. QUALITY MONITORING

Figure 19: Overview of globally distributed “fiducial” AOIs/tiles used as the basis for monitoring the quality of Planet Fusion and for validating new releases.



A set of geographically distributed “fiducial” AOIs ([Figure 19](#)) are used as the basis for monitoring the quality of Planet Fusion and for validating new releases. These reference AOIs were selected to cover a variety of surface types, land surface topographical features, and cloud environments to effectively “stress” test new releases, ensure that code refinements and new features do not negatively impact quality metrics, identify/correct edge case issues, and provide a robust foundation for tracking progress in radiometric and geometric performance.

The following sub-sections provide assessments of the performance of the Planet Fusion surface reflectance product related to radiometric and geometric harmonization, cloud masking, and gap-filling. We are constantly working to improve and expand the validation and quality monitoring processes to further improve the product and provide transparent insights into the quality of the product.

### 5.1. RADIOMETRIC VALIDATION

[Figure 20](#) illustrates the CESTEM-based radiometric harmonization results on a specific date for two AOIs in California (top) and Nebraska (bottom). The harmonization is able to robustly re-calibrate the PlanetScope input stream, producing Planet Fusion (PF-SR) NDVI values that align well with day-coincident FORCE-based L8/S-2 NDVI with a mean absolute difference (MAD) of ~4%. Noteworthy, is the bimodal distribution of the PlanetScope based NDVI relative to L8, which results from having sensors with different spectral bands and relative spectral responses featured in the tile. This showcases the promise of the CESTEM approach for accounting for such non-linearities in spectral associations between the input and reference (i.e., L8 or S-2) stream. While CESTEM

can ensure radiometric consistency with the chosen “gold reference” (i.e., FORCE), a perfect 1:1 agreement will not always be guaranteed. This results from the advanced Planet Fusion “clean up” process involving 1) enhanced cloud and cloud shadow detection ([Section 4.3](#)), 2) multi-sensor and multi-time reference sampling ([Section 4.4](#)), and 3) temporal filtering ([Section 4.7](#)), which effectively minimizes uncertainties (e.g., due to atmospheric contamination, BRDF effects, calibration inaccuracies) impacting both the PlanetScope and Landsat/S-2 data streams. As a result, Planet Fusion data will in general be characterized by enhanced radiometric robustness and spatio-temporal consistency.

Figure 20: Quality (relative to L8/S-2) of the Planet Fusion (PF-SR) NDVI harmonization process showcased for two regions with day-coincident PlanetScope and L8/S-2 acquisitions

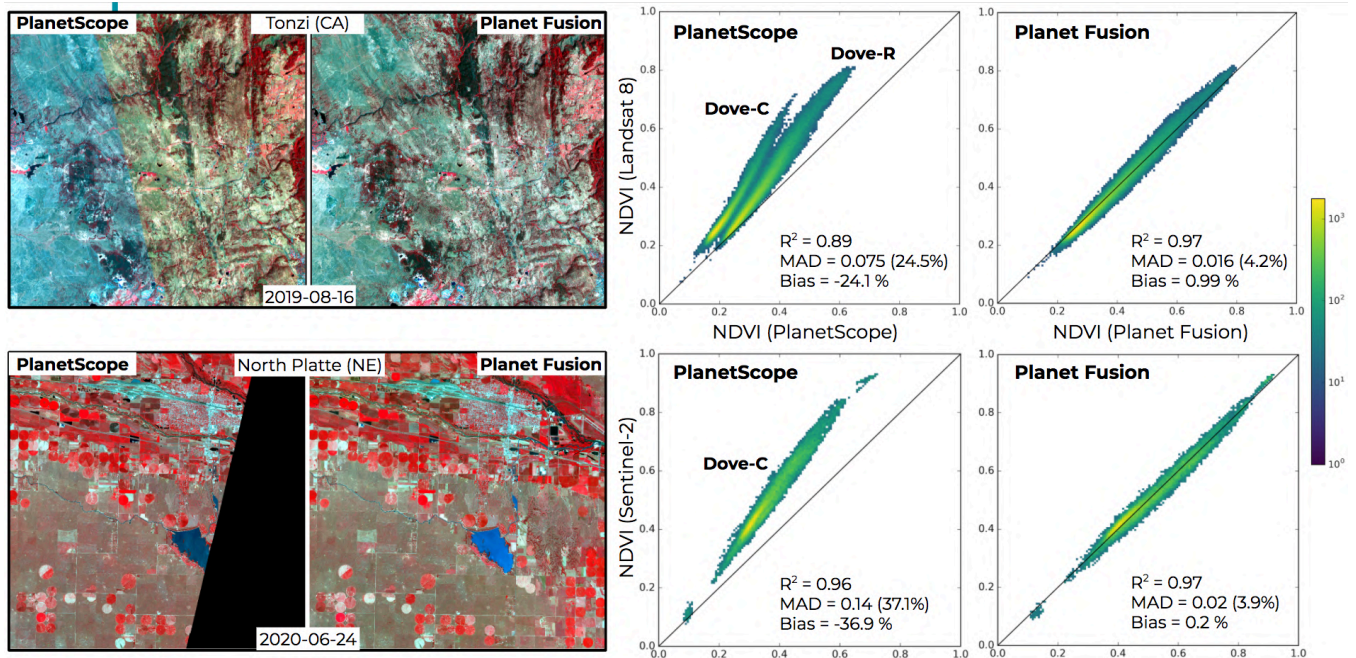


[Figure 21](#) depicts the results of a more extensive multi-version (release 1.2.5 vs 1.3.0) comparison of all available (i.e., satisfying a 50% clear-sky threshold) FORCE images against day-coincident CSTEM-SR product artifacts (i.e., before gap-filling and temporal filtering) over the Brazil fiducial AOI (22S/18E-33S) ([Figure 19](#)). The density scatter plots indicate highly correlated datasets with R<sup>2</sup> values of ~0.99 for all 4 spectral bands. Release 1.3.0 constitutes an improvement over the previous release with overall mean absolute difference (MAD) percentages ranging from 1.29% (NIR) to 3.15% (blue) relative to 1.80% (NIR) to 4.11% (blue) for release 1.2.5. Mean bias (MB) percentages are generally low with the overall MB below ~1% for all bands. Mean binned statistics (MAD and MB) accompany the density scatter plots to help illustrate/detect any trends in the radiometric performance relative to FORCE. In general the MAD percentages are slightly higher for low reflectance values although that trend is less obvious in release 1.3.0.

The FORCE - CSTEM-SR comparison statistics for the majority of the fiducial AOIs are summarized in [Table 7](#). Noteworthy is the consistent across the board improvement in performance (i.e., agreement with FORCE) in release 1.3.0 relative to release 1.2.5. The best performances (high R<sup>2</sup>, low MAD) are observed in AOIs dominated by agriculture (Nebraska, Brazil, Egypt) with band-specific MADs ranging from 1.29% to 4.81% (release 1.3.0). AOIs with a majority of mostly “invariant” surface features such as Railroad Valley in Nevada (11N/25E-177N) and Madagascar (tropical forest) (39S/12E-342N) are also performing well with MADs ~2%. We are seeing a significant improvement over the water dominated Egypt tile (36N/10E-144N, [Figure 19](#)) in release 1.3.0, with the MAD of the red band decreasing from 17.33% to 5.55%. This is related to an issue with the radiometric calibration in tiles with significant water bodies in release 1.2.5, which has been effectively resolved in release 1.3.0. This is a testimony of

the value of the fiducial radiometric quality monitoring in verifying and quantifying the impact of code refinements such as this.

Figure 21:: Clear-sky FORCE vs CESTEM (CSTEM-SR) surface reflectance comparison for the Brazil (22S/18E-33S) fiducial AOI based on imagery acquired/produced between 2021-07-01 to 2023-05-14. Results are shown for two different Fusion releases (1.2.5 vs 1.3.0).

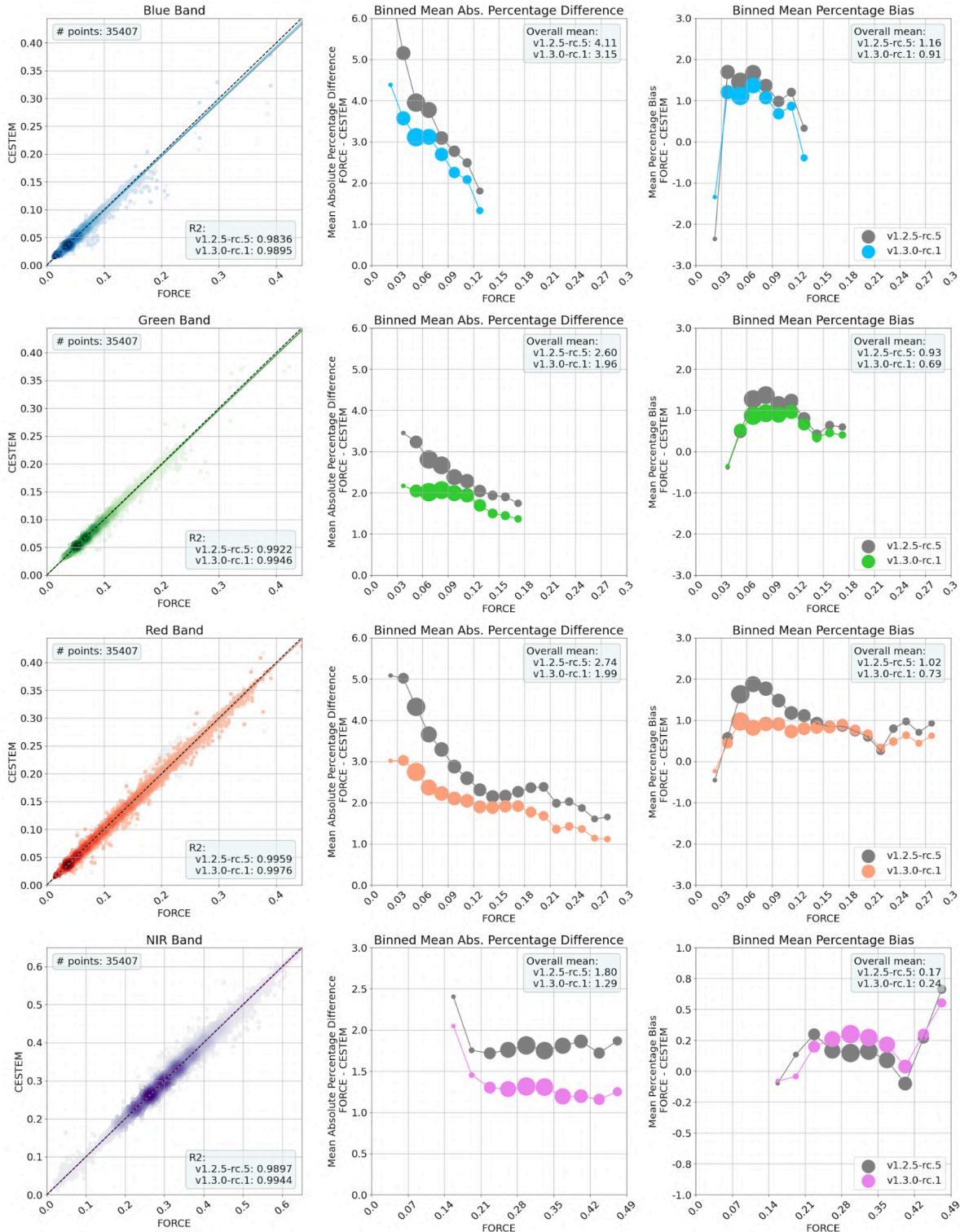


Table 7: FORCE vs CSTEM-SR surface reflectance comparison statistics for 10 (1.2.5 results not available for the remaining 5 AOIs) of the fiducial AOIs (Figure 19) over the fiducial backfill TOI (2021-07-01 to 2023-05-14). Results are shown for two different Fusion releases (1.2.5 vs 1.3.0) and the best performing statistics are in bold. These results are based on backfill (BF) data alone.

FORCE vs CSTEM SR evaluation (BF)				R2		MAD [%]		Bias [%]	
Tile ID	Location	Samples	Band	1.2.5	1.3.0	1.2.5	1.3.0	1.2.5	1.3.0
10N/24E-188N	California	62595	Blue	0.821	<b>0.916</b>	13.01	<b>9.28</b>	4.08	<b>2.29</b>
			Green	0.881	<b>0.946</b>	9.47	<b>6.35</b>	2.80	<b>1.54</b>
			Red	0.936	<b>0.971</b>	9.52	<b>6.45</b>	2.76	<b>1.53</b>
			NIR	0.691	<b>0.867</b>	8.97	<b>5.57</b>	1.83	<b>1.17</b>
11N/25E-177N	Nevada	62939	Blue	0.917	<b>0.968</b>	4.66	<b>2.63</b>	0.75	<b>0.37</b>
			Green	0.928	<b>0.971</b>	4.13	<b>2.44</b>	0.68	<b>0.34</b>
			Red	0.930	<b>0.972</b>	3.65	<b>2.11</b>	0.56	<b>0.27</b>
			NIR	0.926	<b>0.969</b>	3.29	<b>1.92</b>	0.50	<b>0.25</b>
14N/28E-189N	Nebraska	68145	Blue	0.934	<b>0.958</b>	6.24	<b>4.81</b>	1.05	<b>1.03</b>
			Green	0.967	<b>0.979</b>	3.96	<b>2.99</b>	0.79	<b>0.78</b>
			Red	0.990	<b>0.993</b>	3.15	<b>2.45</b>	0.70	<b>0.56</b>
			NIR	0.991	<b>0.994</b>	2.08	<b>1.60</b>	<b>0.12</b>	0.25
14N/29E-189N	Nebraska	56472	Blue	0.951	<b>0.964</b>	5.43	<b>4.51</b>	<b>0.80</b>	1.11
			Green	0.972	<b>0.980</b>	3.60	<b>2.89</b>	<b>0.59</b>	0.79
			Red	0.990	<b>0.993</b>	2.84	<b>2.24</b>	<b>0.51</b>	0.55
			NIR	0.985	<b>0.990</b>	1.84	<b>1.40</b>	<b>0.01</b>	0.20
22S/18E-335N	Brazil	35407	Blue	0.984	<b>0.990</b>	4.11	<b>3.15</b>	1.16	<b>0.91</b>
			Green	0.992	<b>0.995</b>	2.60	<b>1.96</b>	0.93	<b>0.69</b>
			Red	0.996	<b>0.998</b>	2.74	<b>1.99</b>	1.02	<b>0.73</b>
			NIR	0.990	<b>0.994</b>	1.80	<b>1.29</b>	<b>0.17</b>	0.24
36N/10E-144N	Egypt	34311	Blue	0.945	<b>0.980</b>	7.33	<b>3.93</b>	1.31	<b>0.89</b>
			Green	0.957	<b>0.984</b>	5.28	<b>2.78</b>	0.75	<b>0.64</b>
			Red	0.976	<b>0.990</b>	5.64	<b>3.10</b>	0.86	<b>0.68</b>
			NIR	0.992	<b>0.997</b>	2.31	<b>1.42</b>	0.23	<b>0.20</b>
36N/10E-145N	Egypt	16428	Blue	0.757	<b>0.941</b>	13.52	<b>4.53</b>	2.67	<b>1.69</b>
			Green	0.807	<b>0.955</b>	13.75	<b>4.46</b>	2.20	<b>1.70</b>
			Red	0.891	<b>0.974</b>	17.33	<b>5.55</b>	3.02	<b>2.23</b>
			NIR	0.970	<b>0.993</b>	12.88	<b>4.47</b>	3.51	<b>1.69</b>
32N/28E-217N	Austria	16127	Blue	0.919	<b>0.955</b>	11.89	<b>7.58</b>	2.74	<b>0.72</b>
			Green	0.935	<b>0.972</b>	9.53	<b>5.69</b>	2.17	<b>0.50</b>
			Red	0.949	<b>0.979</b>	10.35	<b>6.14</b>	3.07	<b>0.73</b>
			NIR	0.837	<b>0.947</b>	7.94	<b>4.01</b>	0.95	<b>0.22</b>
52N/20E-211N	China	43738	Blue	0.977	<b>0.983</b>	9.41	<b>7.69</b>	4.67	<b>4.08</b>
			Green	0.985	<b>0.991</b>	7.23	<b>5.23</b>	1.82	<b>1.54</b>
			Red	0.984	<b>0.990</b>	6.90	<b>5.10</b>	2.86	<b>2.35</b>
			NIR	0.983	<b>0.990</b>	5.63	<b>3.91</b>	1.06	<b>0.95</b>
39S/12E-342N	Madagascar	1350	Blue	0.982	<b>0.985</b>	2.50	<b>2.11</b>	<b>-0.24</b>	-0.59
			Green	0.973	<b>0.988</b>	2.07	<b>1.25</b>	<b>0.08</b>	-0.14
			Red	0.989	<b>0.991</b>	2.53	<b>1.69</b>	<b>-0.14</b>	-0.17
			NIR	0.924	<b>0.975</b>	2.40	<b>1.43</b>	<b>-0.18</b>	-0.21

The largest differences between FORCE and CSTEM-SR are observed over the mountainous AOIs in California (10N/24E-188N) and Austria (32N/28E-217N) (Table 7). These AOIs are characterized by significant topography, mountain snow, and complex weather. Starting with release 1.3.0, the PlanetScope based product artifacts produced in the Fusion pipeline are corrected for the effects of topography on reflectance (Section 4.2), which is shown to improve the agreement with FORCE by 3 - 4 percentage points with a significant reduction in biases.

As previously mentioned, the Planet Fusion radiometric harmonization approach will attempt to minimize the impact of uncertainties in the FORCE data arising from residual cloud contamination, atmospheric correction uncertainties, and BRDF effects. As such, care should be taken in considering the FORCE data as a source of truth for validation purposes. [Figure 22](#) showcases three dates with considerable reflectance differences between coincident FORCE and CSTEM-SR, which are contributing to the relatively high MADs (5 - 9%) reported for the California AOI ([Table 7](#)). The biggest differences occur on sloping terrain that show up as very bright in the FORCE imagery on 2021-10-04 and 2022-09-15, whereas other topography related artifacts are evident on 2023-02-15. In these cases, the interactions between the topography and sensor view and sun illumination geometries are introducing significant uncertainties in the FORCE data, which we don't want to inherit as part of the CESTEM calibration approach. The corresponding CSTEM-SR images are predominantly free of these artifacts, supporting the notion of Planet Fusion generally being characterized by enhanced radiometric robustness and spatio-temporal consistency relative to the original FORCE data.

Over the China fiducial AOI (52N/20E-211N) widespread snow early and late in the year is responsible for the relatively high overall MADs (4 - 7%) as the snow signal is generally more stable (less fluctuating) over time in the Planet Fusion imagery, which may be a result of the multi-temporal reference sampling approach as well as reduced BRDF effects in PlanetScope imagery.

Figure 22: Comparison of day-coincident FORCE and CSTEM-SR imagery (natural color RGB) within the California fiducial AOI on dates with significant reflectance differences. The differences are mainly attributed to issues with the FORCE data due to terrain and view geometry induced "brightness" artifacts.

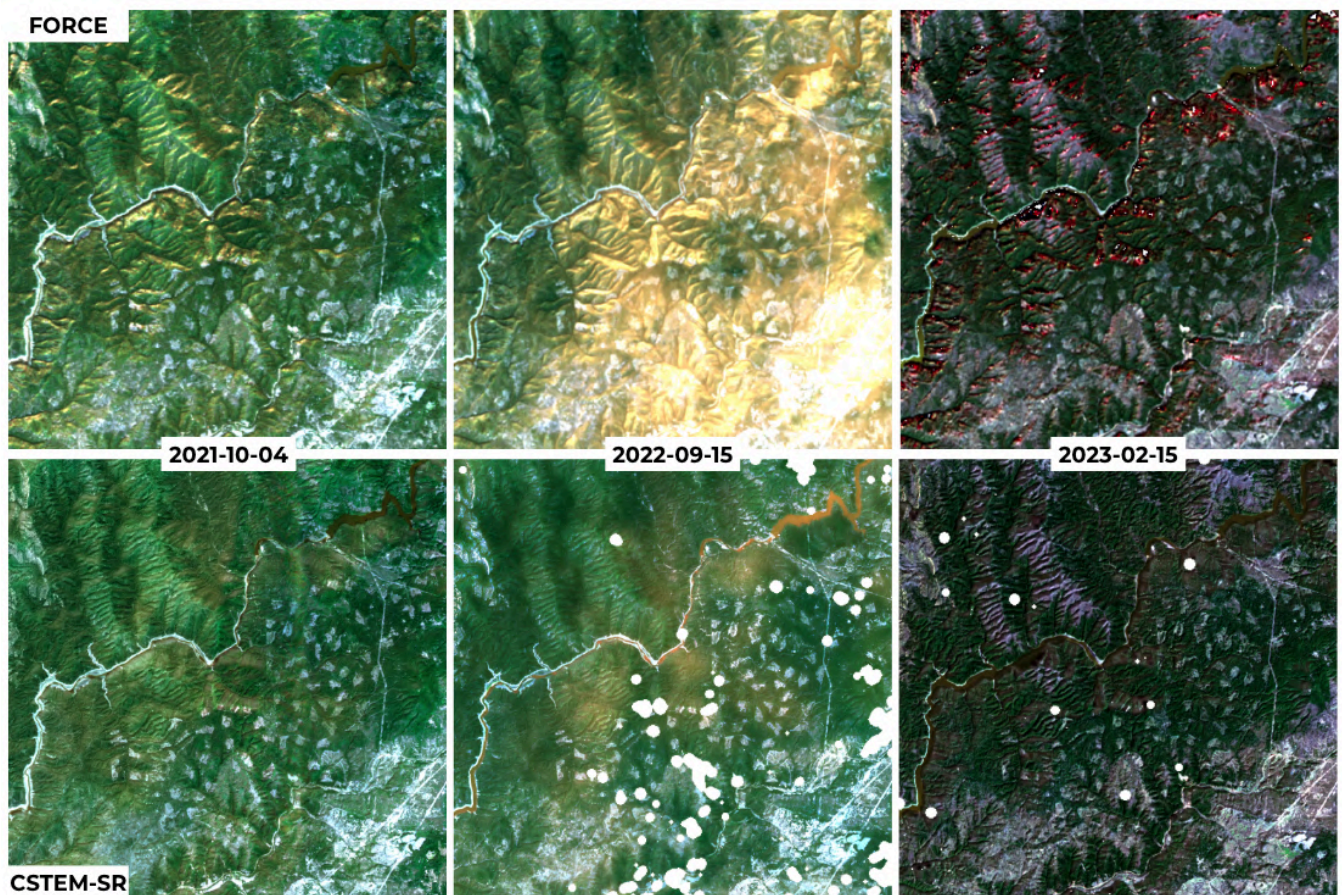


Table 8: FORCE vs CSTEM-SR surface reflectance comparison statistics over the fiducial single-step forward-fill TOI (2023-05-15 to 2023-06-15). Results are shown for two different Fusion releases (1.2.5 vs 1.3.0) and the best performing statistics are in bold. Note that these results are based on forward-fill (FF) data alone and not all of the fiducial AOIs had sufficient FORCE data to satisfy the 50% clear-sky threshold condition.

FORCE vs CSTEM SR evaluation (FF)				R2		MAD [%]		Bias [%]	
Tile ID	Location	Samples	Band	1.2.5	1.3.0	1.2.5	1.3.0	1.2.5	1.3.0
10N/24E-188N	California	2697	Blue	<b>0.910</b>	0.894	<b>6.43</b>	6.99	1.45	<b>1.12</b>
			Green	0.789	<b>0.883</b>	6.63	<b>4.76</b>	4.45	<b>1.90</b>
			Red	0.960	<b>0.962</b>	6.27	<b>5.75</b>	2.44	<b>1.17</b>
			NIR	0.706	<b>0.884</b>	7.85	<b>4.99</b>	7.02	<b>4.00</b>
11N/25E-177N	Nevada	2523	Blue	0.748	<b>0.790</b>	6.41	<b>6.06</b>	<b>-4.28</b>	-4.41
			Green	0.774	<b>0.843</b>	5.41	<b>4.67</b>	-2.97	<b>-2.59</b>
			Red	0.795	<b>0.843</b>	4.79	<b>4.23</b>	-2.86	<b>-2.59</b>
			NIR	0.762	<b>0.830</b>	4.60	<b>3.84</b>	-1.02	<b>-0.97</b>
14N/28E-189N	Nebraska	1192	Blue	<b>0.920</b>	0.915	<b>5.28</b>	5.49	<b>-0.99</b>	-2.83
			Green	0.903	<b>0.911</b>	5.30	<b>5.21</b>	<b>-3.74</b>	-4.07
			Red	0.929	<b>0.941</b>	6.67	<b>6.13</b>	-5.79	<b>-5.32</b>
			NIR	0.907	<b>0.917</b>	4.85	<b>4.54</b>	0.94	<b>0.89</b>
14N/29E-189N	Nebraska	2542	Blue	<b>0.860</b>	0.833	<b>4.45</b>	5.27	<b>-0.37</b>	-3.41
			Green	<b>0.880</b>	0.856	<b>3.84</b>	4.37	<b>-0.92</b>	-2.57
			Red	<b>0.914</b>	0.899	<b>4.21</b>	4.62	<b>-2.57</b>	-3.20
			NIR	<b>0.622</b>	<b>0.622</b>	<b>4.01</b>	4.06	2.34	<b>1.64</b>
22S/18E-335N	Brazil	2950	Blue	<b>0.936</b>	0.915	<b>6.10</b>	6.22	1.37	<b>-0.11</b>
			Green	<b>0.946</b>	0.938	<b>4.99</b>	5.00	1.30	<b>0.22</b>
			Red	<b>0.972</b>	0.964	7.18	<b>6.62</b>	2.85	<b>0.75</b>
			NIR	0.972	<b>0.982</b>	2.81	<b>2.14</b>	-2.19	<b>-1.27</b>
52N/20E-211N	China	1200	Blue	0.882	<b>0.907</b>	9.95	<b>8.13</b>	-4.43	<b>-1.07</b>
			Green	0.881	<b>0.929</b>	8.66	<b>6.39</b>	-4.76	<b>-2.28</b>
			Red	0.889	<b>0.932</b>	13.06	<b>10.06</b>	-9.91	<b>-7.56</b>
			NIR	0.959	<b>0.968</b>	7.34	<b>6.82</b>	<b>0.20</b>	-1.02

Table 8 reports FORCE versus CSTEM-SR comparison statistics based on forward-fill data alone. The TOI for the fiducial release validation includes a 1 month forward-fill period (2023-05-15 to 2023-06-15) during which a simulated “single-step” forward-fill operation is deployed to closely resemble true forward-fill conditions (i.e., when running Planet Fusion in near real-time). Given the relatively short forward-fill period, not all of the fiducial AOIs had sufficient FORCE data available to satisfy the 50% clear-sky threshold condition, and in general only a few FORCE scenes were available over each of the AOIs to perform the evaluation. This fact may explain the generally higher MADs and Biases (relative to the backfill analyses) as the aforementioned uncertainties associated with the FORCE data are less likely to factor out (e.g., the high MAD and Bias of the red band over the China AOI was traced back to high uncertainties in the FORCE atmospheric correction).

## 5.2. GEOMETRIC VALIDATION

The geometric performance is based on three key performance indicators (Table 9 - 11) evaluated on a large sample of Planet Fusion images (PF-SR) produced for the fiducial AOIs (Figure 19) over the full period of the fiducial TOI (2021-07-01 to 2023-05-14). Detailed information on the geometric accuracy assessment protocols and reference imagery sources are provided in Planet Team 2023. Absolute positional accuracy (ABS) measures how accurately objects are positioned on the image in respect to their true position on the ground. For the most recent release (1.2.5), ABS is characterized by an average Root Mean Square Error (RMSE) of 2.80 m (Table 9) where the average RMSE is the average of the RMSEs for each individual image (sample) evaluated within the

fiducial AOIs. The PCTL90/95 of RMSE metrics define the 90/95th percentile of the individually measured RMSEs, which suggests that 90% of the evaluated PF-SR images have an RMSE of  $\leq 4.80$  m. Noteworthy is the improvement trend in ABS between the releases with 1.2.5 performing better across all statistical metrics.

Table 9: Planet Fusion absolute positional accuracy statistics for different release versions based on tile-level images from 10 of the fiducial AOIs (the 5 remaining AOIs were introduced in v1.3.0). The best performing statistics are in bold.

Version	Sample Size	Avg RMSE (m)	PCTL90 of RMSE (m)	PCTL95 of RMSE (m)	Max RMSE (m)	STD RMSE (m)
1.2.5	7,027	<b>2.80</b>	<b>4.80</b>	<b>5.75</b>	<b>9.25</b>	<b>1.44</b>
1.2.4	3,626	2.91	5.69	6.78	11.12	1.81
1.1.7	3,383	3.34	6.66	8.07	10.96	2.12
1.1.2	3,574	4.73	8.76	10.86	15.96	2.96

Band to band alignment (B2B) is a measure of how accurately the different bands in the image are aligned relative to each other. In release 1.2.5 sub-pixel accuracy in B2B is retrieved with 95% of the evaluated images being characterized by an RMSE of 0.55 m or better ([Table 10](#)). This performance indicator has seen significant improvement across the shown release versions.

Table 10: Planet Fusion band to band alignment statistics for different release versions based on tile-level images from 10 of the fiducial AOIs (the 5 remaining AOIs were introduced in v1.3.0). The best performing statistics are in bold.

Version	Sample Size	Avg RMSE (m)	PCTL90 of RMSE (m)	PCTL95 of RMSE (m)	Max RMSE (m)	STD RMSE (m)
1.2.5	13,050	<b>0.33</b>	<b>0.46</b>	<b>0.55</b>	29.51	<b>0.79</b>
1.2.4	19,961	0.64	1.57	2.16	29.10	1.03
1.1.7	19,222	1.08	4.69	5.84	<b>12.41</b>	1.38
1.1.2	19,003	2.19	5.97	8.23	19.78	2.84

Temporal registration (TEMP) is a measure of how well images acquired/produced over the same AOI align in time. This performance indicator is currently being evaluated using the first image in the temporal stack as the “anchor” image. The Planet Fusion images are generally very well aligned temporally with an average sub-pixel TEMP accuracy of 1.57 m for release 1.2.5 ([Table 11](#)). This suggests that the adopted “bundle-adjustment” approach ([Section 4.5](#)) is working as expected.

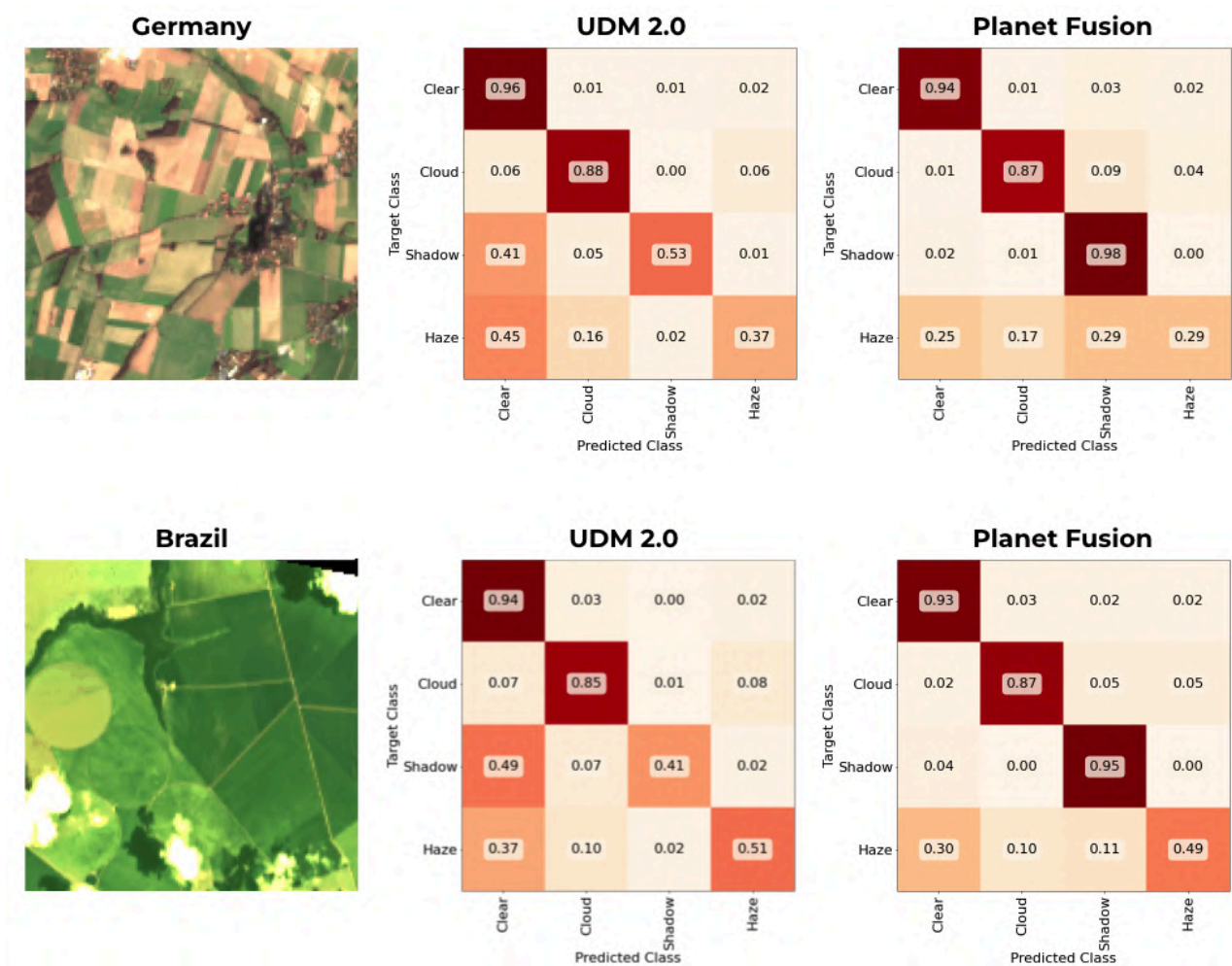
Overall the three geometric performance indicators provide confidence in the robustness and validity of the applied geometric harmonization with sub-pixel ( $< 3$  m) accuracy retrieved for the large majority of images. These assessments were done at the tile-level and may not always be a good representation of the sub-tile (more localized) geometric performance. It is also worth stressing that Planet Fusion derived geometric shifts adjustments are “global” in nature (i.e., the same shift is applied to all pixels in a given image/scene), and as such can’t correct for intra-image/intra-scene geometric distortions present in the native PlanetScope imagery.

Table 11: Planet Fusion temporal registration statistics for different release versions based on tile-level images from to of the fiducial AOIs (the 5 remaining AOIs were introduced in v1.3.0). The best performing statistics are in bold.

Version	Sample Size	Avg RMSE (m)	PCTL90 of RMSE (m)	PCTL95 of RMSE (m)	Max RMSE (m)	STD RMSE (m)
1.2.5	6,589	<b>1.57</b>	<b>3.48</b>	<b>4.01</b>	9.06	<b>1.3</b>
1.2.4	3,541	2.65	5.62	7.58	12.83	2.58
1.1.7	2,860	2.26	4.89	5.28	<b>7.39</b>	1.61
1.1.2	2,752	5.7	13.83	16.45	24.62	5.48

### 5.3. CLOUD MASK PERFORMANCE

Figure 23: Confusion matrices for UDM 2.0 (middle column) and Planet Fusion (right column) cloud-masks for validation chips (left column) in Germany (top row) and Brazil (bottom row).



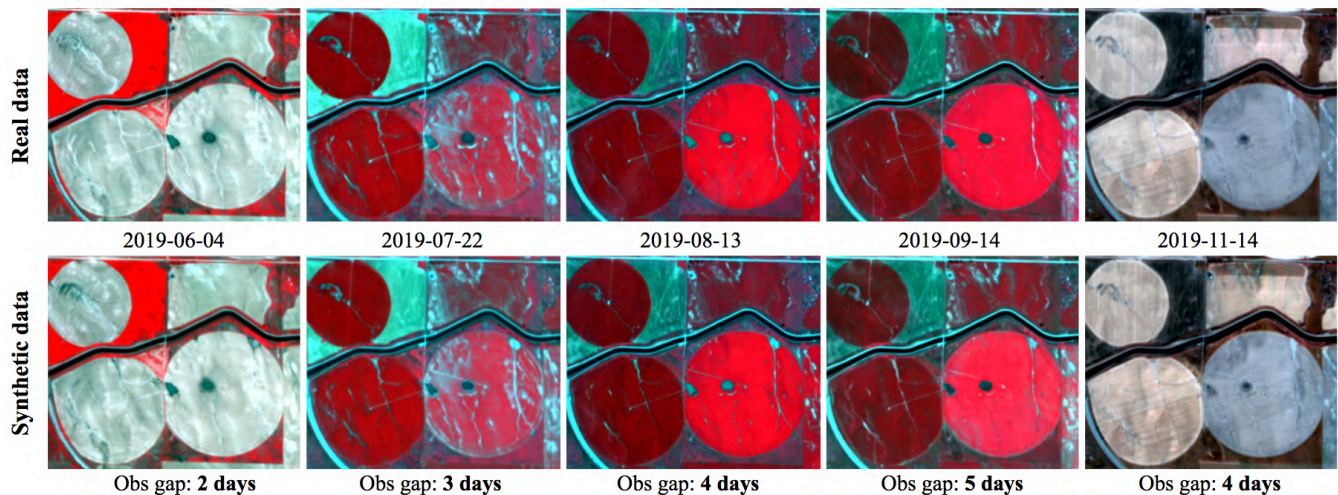
As part of a preliminary assessment of the cloud masking performance, hand-labeled cloud masks were curated for smaller chips (4.5 x 4.5 km) within select AOIs. The labels were generated based off of 3 m PlanetScope TOAR

data and each pixel was labeled as either clear, cloud, cloud shadow, snow, or haze. [Figure 23](#) depicts initial results for two regions in Germany and Brazil. Confusion matrices were computed for both Planet Fusion and UDM 2.0 (i.e., the cloud mask distributed alongside standard PS data and used as the primary initial cloud mask in Planet Fusion processing) using the overlapping classes (clear, cloud, cloud shadow, haze). From these confusion matrices we see a significant improvement to cloud masking (reduced omission/commission errors) with Planet Fusion relative to UDM 2.0. Improvements are particularly noticeable for the cloud shadow class that are mis-classified for 47 % (Germany) and 59% (Brazil) of the pixels in UDM 2.0 whereas Planet Fusion reports a 98% (Germany) and 95% (Brazil) correct classification. UDM 2.0 is more prone to omission issues with 6% (Germany) and 7% (Brazil) of the cloud pixels mis-classified as clear, in comparison to 1% (Germany) and 2% (Brazil) for Planet Fusion. While Planet Fusion also performs better for the haze class, omission errors are still significant, which highlights the challenges associated with accurate haze detection. These results are preliminary and based on a relatively small sample size (only two AOIs). We also need to consider a certain amount of uncertainty in the hand-labeled cloud masks, as they are not always accurate. Furthermore it should be noted that UDM 2.1 constitutes an improvement over UDM 2.0 and is applied to PlanetScope imagery acquired after 2023-11-21.

Cloud masking is notoriously difficult and a balancing battle between omission (detecting too much) and commission (detecting too little) issues. While the Planet Fusion cloud scheme is slightly more “aggressive” compared to UDM 2.0 ([Figure 23](#)), elaborate cloud verification steps are in place to significantly reduce cloud commission errors ([Section 4.3](#)). As highlighted in [Section 4.7](#), residual cloud contamination (omission issues) in the intermediate cloud-masked images (CSTEM-SR) will oftentimes be detected as outliers during the temporal filtering step and therefore will typically not feature in the final product artifacts. Furthermore, the elaborate temporally-driven CESTEM-based radiometric calibration approach ([Section 4.4](#)) will often reduce the impact of any undetected haze in the imagery.

## 5.4. GAP-FILLING PERFORMANCE

Figure 24: Observed (real) versus gap-filled (synthetic) Planet Fusion data for different observation gap intervals (false color: NIR, Red, Green)



Users are advised to consult with the included QA metrics ([Table 5](#)) to determine the retrieval confidence of the gap-filled (synthetic) pixel values. [Figure 24](#) provides a visual demonstration of the fidelity of the gap-filled data values for different observation gaps over an agricultural region in Nebraska. In general, the fine-scale features and reflectance magnitudes in the actual data (top panel) are accurately reproduced in the synthetic data

(bottom panel). However, as the observation gap increases further you are likely to see greater reflectance discrepancies, particularly if surface conditions change in a non-linear fashion. However, given the availability of near-daily PlanetScope imaging, the acquisition/observation gaps between clear-sky images will often be within reasonable limits over the majority of landscapes and environments.

Figure 25: Box-and-whisker plots of red (top) and NIR (bottom) band relative [%] mean absolute differences (MAD) between gap-filled and observed pixel values as a function of the day gap (binned) to the observed data. Results were compiled from Fusion back-fill (left) and forward-fill (right) runs over a wide variety of geographies (Figure 19) with day gaps ranging from 1 to ~200 days. The full box-and-whisker statistics and provided below each plot.

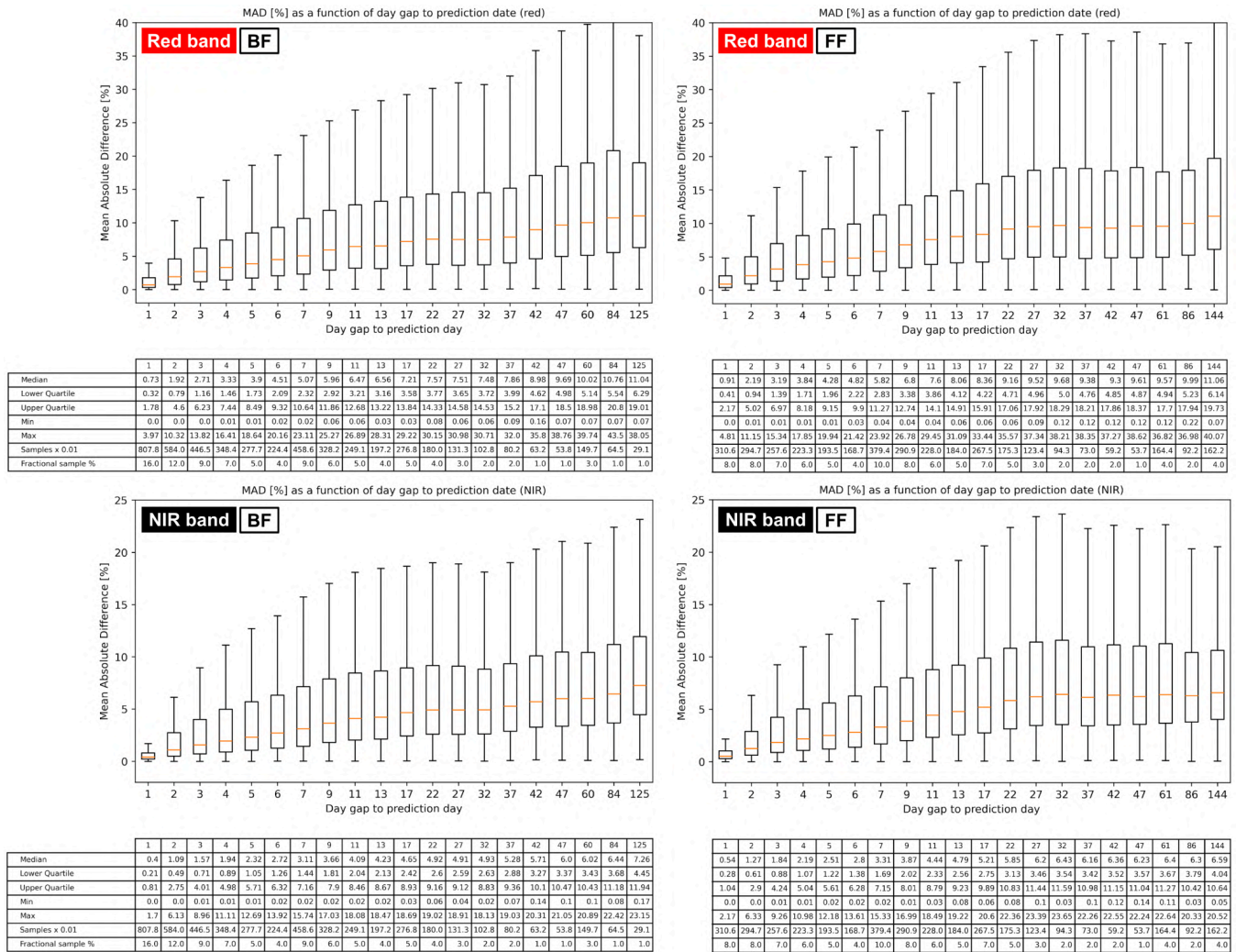


Figure 25 shows box-and-whisker representations of band-specific relative MADs between gap-filled and observed data as a function of the observation gap, which was compiled from the geographically diverse dataset used to train the confidence models (Section 4.8). These plots display the minimum, lower quartile, median, upper quartile, and maximum MAD across a wide range in the observation gaps (1 - ~200 days) and results were compiled from both backfill (BF) and forward-fill (FF) Fusion runs. The FF statistics are based on runs with no forward look and as such provide an approximation of gap-filling uncertainties when only historic data (relative to the prediction date) is available. Not surprisingly, FF is associated with larger uncertainties relative to BF up till an observation gap of ~47 days where the red (NIR) band relative median MADs plateau at around 10% (6%). In BF (FF), the median MAD shows an increasing trend from 0.73% (0.91%) to 7.57% (9.16%) for the red band and 0.4% (0.54%) to 4.92% (5.85%) for the NIR band as the observation gap increases from 1 to 22

days. The upper quartiles of MAD show similar trends peaking at around 20% (11%) for the red (NIR) band in both BF and FF mode. The max values (the whiskers) correspond to the 100th percentile excluding outliers (i.e., points that fall outside the upper quartile + 1.5 x the interquartile range) and range from around 4% (1.7%) to 44% (23%) for the red (NIR) band. The distribution of the samples across the day gap bins is notably different between BF and FF ([Figure 25](#)). In BF (FF), the day gap to the prediction day is  $\leq 5$  days for 49% (34%) of the samples, and 10% of the FF samples have a day gap  $\geq 60$  days compared to only 5% of BF samples.

## 6. KNOWN LIMITATIONS AND CAVEATS

- **False cloud/shadow detections** may occur in certain cases: 1) if surface conditions change very rapidly, 2) during prolonged cloudiness, or 3) over AOIs with complex terrain and shadowing. Significant effort has gone into developing automated techniques to differentiate between actual change and atmospheric contamination, but in some cases commission errors can still be an issue.
- **Gap-filling artifacts** may occur over water and during periods of 1) prolonged cloudiness and 2) snow.
- Planet Fusion is not well-suited for the identification of **short-lived** (i.e., less than 1 - 2 days) **surface features** (e.g., moving vehicles/ships, erection of temporary shelters, flash floods), which may appear as anomalies and undergo smoothing during the temporal filtering step ([Section 4.7](#)).
- **Planet Fusion is not suited for studies over snow covered surfaces.** As it is virtually impossible to robustly distinguish between snow and clouds based on 4-band VNIR data, periodic snow cover will in most cases be masked out as clouds. Snow covered scenes will be down-prioritized during gap-filling as the mixing of spectral signals from snow and no snow conditions can introduce severe artifacts. As a result, Planet Fusion reproduced surface reflectance signals may be associated with large uncertainties during times when snow is expected. It also means that occasionally you may see very large observational lags (QA layer 2, [Table 5](#)) as the gap-filling algorithm has difficulty identifying a snow free scene.
- As the Fusion processing is done independently for each tile, **tile boundary artifacts** can sometimes occur when doing cross-tile analyses. This may be manifested in the form of typically small inter-tile brightness differences and sub-pixel mis-alignments. These artifacts will tend to be more prevalent for gap-filled data.
- **Forward-fill** data will typically be associated with larger uncertainties relative to **Backfill** data. This is particularly the case during periods of extended gap-filling and for “atypical” change events (e.g., disturbances).
- The current Planet Fusion product suite is **4-bands only**. The general framework is extendable to other spectral bands and a red-edge band is expected to become available within the foreseeable future.
- Lastly, the notion of a perfect product is utopian. Remote sensing is hard. Cloud masking is a balancing act and an unwinnable battle between commission and omission errors. Gap-filling, and forecasting in particular, is an inherently ill-posed problem and only works well when change is “typical” and associated with past dynamics. There WILL be cases where Planet Fusion doesn't perform as well as we want it to. A lot of effort has gone into developing a differentiated next generation surface reflectance product with an ambition to be “best in class”. We are committed to continuously improving it towards realizing the promise of high fidelity, timely, usable, and actionable insights from multi-source satellite observations.

## REFERENCES

- B. Aragon, M.G. Ziliani, R. Houborg, T.E. Frantz. 2021. CubeSats deliver new insights into agricultural water use at daily and 3 m resolutions. *Sci Rep* 11, 12131. <https://doi.org/10.1038/s41598-021-91646-w>
- M. Claverie, J. Ju, J.G. Masek, J.L. Dungan, E.F. Vermote, J.-C. Roger, S.V. Skakun, C. Justice. 2018. The Harmonized Landsat and Sentinel-2 surface reflectance data set. *Remote Sensing of Environment*, 219, 145-161: <https://doi.org/10.1016/j.rse.2018.09.002>
- G. Doxani, E. Vermote, J.-C. Roger, F. Gascon, S. Adriaensen, D. Frantz, O. Hagolle, A. Hollstein, G. Kirches, F. Li, J. Louis, A. Mangin, N. Pahleva, B. Pflug, Q. Vanhellemont. 2018. Atmospheric Correction Inter-Comparison Exercise. *Remote Sens.*, 10(2), 352: <https://doi.org/10.3390/rs10020352>
- G. Doxani, E.F. Vermote, J.-C. Roger, S. Skakun, F. Gascon, A. Collison, L. De Keukelaere, C. Desjardins, D. Frantz, O. Hagolle, M. Kim, J. Louis, F. Pacifici, B. Pflug, H. Poilvé, D. Ramon, R. Richter, F. Yin. 2023. Atmospheric Correction Inter-comparison eXercise, ACIX-II Land: An assessment of atmospheric correction processors for Landsat 8 and Sentinel-2 over land. *Remote Sensing of Environment*, 285, 113412. <https://doi.org/10.1016/j.rse.2022.113412>
- ESA. 2024. The European Space Agency. Available online: <https://sentinels.copernicus.eu/web/sentinel/user-guides/sentinel-2-msi/resolutions/spatial> (accessed on 12 May 2024)
- D. Frantz. 2019a. FORCE—Landsat + Sentinel-2 Analysis Ready Data and Beyond. *Remote Sensing*, 11, 1124: <https://doi.org/10.3390/rs11091124>
- D. Frantz, M. Stellmes, P.A. Hostert. 2019b. Global MODIS Water Vapor Database for the Operational Atmospheric Correction of Historic and Recent Landsat Imagery. *Remote Sens.*, 11, 257. <https://doi.org/10.3390/rs11030257>
- D. Frantz, E. Haß, A. Uhl, J. Stoffels, J. Hill. 2018. Improvement of the Fmask algorithm for Sentinel-2 images: Separating clouds from bright surfaces based on parallax effects. *Remote Sens. Environ.*, 215, 471–481: <https://doi.org/10.1016/j.rse.2018.04.046>
- R. Houborg, M.F. McCabe. 2018a. Daily Retrieval of NDVI and LAI at 3 m Resolution via the Fusion of CubeSat, Landsat, and MODIS data. *Remote Sensing*, 10(6), 890: <https://doi.org/10.3390/rs10060890>
- R. Houborg, M.F. McCabe. 2018b. A Cubesat Enabled Spatio-Temporal Enhancement Method (CESTEM) utilizing Planet, Landsat and MODIS data. *Remote Sensing of Environment*, 209, 211-226: <https://doi.org/10.1016/j.rse.2018.02.067>
- M. Guizar-Sicairos, S.T. Thurman, J.R. Fienup. 2008. Efficient subpixel image registration algorithms. *Optics Letters* 33, 156-158: <https://doi.org/10.1364/OL.33.000156>
- J. Brinkhoff, R. Houborg, B.W. Dunn. 2022. Rice ponding date detection in Australia using Sentinel-2 and Planet Fusion imagery. *Agricultural Water Management*, 273, 107907. <https://doi.org/10.1016/j.agwat.2022.107907>
- K. Johansen., M.G. Ziliani, R. Houborg et al. 2022. CubeSat constellations provide enhanced crop phenology and digital agricultural insights using daily leaf area index retrievals. *Sci Rep* 12, 5244. <https://doi.org/10.1038/s41598-022-09376-6>
- J. Kong, Y. Ryu, J. Liu, B. Dechant, C. Rey-Sanchez, R. Shortt, D. Szutu, J. Verfaillie, R. Houborg, D.D. Baldocchi. 2022. Matching high resolution satellite data and flux tower footprints improves their agreement in photosynthesis estimates. *Agricultural and Forest Meteorology* Vol. 316, 108878, <https://doi.org/10.1016/j.agrformet.2022.108878>
- J. Kong, Y. Ryu, S. Jeong, Z. Zhong, W. Choi, J. Kim, K. Lee, J. Lim, K. Jang, J. Chun, K.-M. Kim, R. Houborg. 2023. Super resolution of historic Landsat imagery using a dual generative adversarial network (GAN) model with CubeSat constellation imagery for spatially enhanced long-term vegetation monitoring. *ISPRS Journal of Photogrammetry and Remote Sensing*, 200, 1-23, <https://doi.org/10.1016/j.isprsjrs.2023.04.013>
- L. Nieto, R. Houborg, A. Zajdband, A. Jumpasut, P.V.V. Prasad, B.J.S.C. Olson, I.A. Ciampitti. 2022. Impact of High-Cadence Earth Observation in Maize Crop Phenology Classification. *Remote Sensing* 14, no. 3: 469. <https://doi.org/10.3390/rs14030469>
- D. Luo, H.K. Zhang, R. Houborg, L.M.N. Ndekelu, M. Maimaitijiang, K.H. Tran, J. McMaine. 2023. Utility of daily 3 m Planet Fusion Surface Reflectance data for tillage practice mapping with deep learning. *Science of Remote Sensing*, 7, 100085. <https://doi.org/10.1016/j.srs.2023.100085>
- J.W. Rouse, R.H. Hass, J.A. Shell, D. Deering. 1973. Monitoring vegetation systems in the Great Plains with ERTS-1. In: *Third Earth Resources Technology Satellite Symposium*. Washington DC, pp. 309–317

D.P. Roy, H.K Zhang, J. Ju, J.L. Gomez-Dans, P.E. Lewis, C.B. Schaaf, Q. Sun, J. Li, H. Huang, V. Kovalsky. 2016. A general method to normalize Landsat reflectance data to Nadir BRDF Adjusted Reflectance. *Remote Sensing of Environment*, Vol. 176, pp 255–271: <https://doi.org/10.1016/j.rse.2016.01.023>

D.P. Roy, J. Li, H.K. Zhang, L. Yan, H.Huang, Z. Li. 2017. Examination of Sentinel-2A multi-spectral instrument (MSI) reflectance anisotropy and the suitability of a general method to normalize MSI reflectance to nadir BRDF adjusted reflectance. *Remote Sensing of Environment*, Vol. 199, pp 25-38: <https://doi.org/10.1016/j.rse.2017.06.019>

D.P. Roy, H. Huan, R. Houborg, V.S. Martins. 2021. A global analysis of the temporal availability of PlanetScope high spatial resolution multi-spectral imagery. *Remote Sensing of Environment*, Vol. 264, 112586: <https://doi.org/10.1016/j.rse.2021.112586>

C.B. Schaaf, F. Gao, A.H. Strahler, W. Lucht, X. Li, T. Tsang, N.C. Strugnell, X. Zhang, Y. Jin, J.-P. Muller et al. 2002. First operational BRDF, albedo nadir reflectance products from MODIS. *Remote Sens. Environ.*, 83, 135–148: [https://doi.org/10.1016/S0034-4257\(02\)00091-3](https://doi.org/10.1016/S0034-4257(02)00091-3)

D. Tanré, C. Deroo, P. Duhaut, M. Herman, J.J. Morcrette, J. Perbos, P.Y. Deschamps. 1990. Description of a Computer Code to Simulate the Satellite Signal in the Solar Spectrum: The 5S Code. *Int. J. Remote Sens.*, 11, 659–668: <https://doi.org/10.1080/01431169008955048>

M.G. Ziliani, M.U. Altaf, B. Aragon, R. Houborg, T.E. Franz, Y. Lu, J. Sheffield, I. Hoteit, M.F. McCabe. 2022. Early season prediction of within-field crop yield variability by assimilating CubeSat data into a crop model. *Agricultural and Forest Meteorology* Vol. 313, 108736, <https://doi.org/10.1016/j.agrformet.2021.108736>

Z. Zhu, C.E. Woodcock. 2012. Object-Based Cloud and Cloud Shadow Detection in Landsat Imagery. *Remote Sens. Environ.*, 118, 83–94: <https://doi.org/10.1016/j.rse.2011.10.028>

Planet Team, 2023. Planet L1 Data Quality Q4 2023 Report. Status of Calibration and Data Quality for the PlanetScope Constellation, December 2023, Available online at <https://support.planet.com/hc/en-us/articles/360037649554-L1-Data-Quality-Reports-for-the-PlanetScope-Constellation>. Last Accessed: May 13, 2024

S.A. Soenen, D. R. Peddle and C. A. Coburn. 2005. SCS+C: a modified Sun-canopy-sensor topographic correction in forested terrain. *IEEE Transactions on Geoscience and Remote Sensing*, vol. 43, no. 9, pp. 2148-2159: <https://doi.org/10.1109/TGRS.2005.852480>

P.M. Teillet, B. Guindon, D.G. Goodenough. 1982. On the slope-aspect correction of multispectral scanner data. *Canadian Journal of Remote Sensing*, 8 (2), pp. 82-106.